

Possible enhancement of the $e^+e^- \rightarrow H^\pm W^\mp$ cross section in the two-Higgs-doublet model

Shinya Kanemura

*Institut für Theoretische Physik der Universität Karlsruhe
D-76128 Karlsruhe, Germany*¹

Abstract

The production process of the charged Higgs-boson associated with a W boson at electron-positron colliders is discussed in the two-Higgs-Doublet Model (2HDM) and in the Minimal Supersymmetric Standard Model (MSSM). The process is induced at one-loop level in these models. We examine how much the cross section can be enhanced by quark- and Higgs-loop effects. In the non-SUSY 2HDM, in addition to large top-bottom (t - b) loop effects for small $\tan\beta$ ($\ll \sqrt{m_t/m_b}$), the Higgs-loop diagrams can contribute to the cross section to some extent for moderate $\tan\beta$ values. For larger $\tan\beta$ ($\gg \sqrt{m_t/m_b}$), such enhancement by the Higgs non-decoupling effects is bounded by the requirement for validity of perturbation theory. In the MSSM with heavy super-partner particles, only the t - b loops enhance the cross section while Higgs-loop effects are very small.

PACS: 12.60.Fr; 14.80.Cp

Keywords: Charged Higgs Bosons, Two Higgs Doublet Models

To appear in European Physical Journal C

¹e-mail: kanemu@particle.physik.uni-karlsruhe.de

1 Introduction

The Higgs sector has not yet been confirmed experimentally. In near future a neutral Higgs boson may be discovered at Tevatron II or LHC, by which the standard picture of particle physics may be completed. The exploration of additional Higgs bosons will be then very important in order to confirm extended Higgs sectors from the minimal Higgs sector in the Standard Model (SM). Actually various theoretical insights suggest such extensions; the supersymmetry (SUSY), extra CP-violating phases, a source of neutrino masses, a remedy for the strong CP problem and so on. Most of the extended Higgs models include charged and CP-odd Higgs bosons. Therefore discovery of a charged Higgs boson, H^\pm , or a CP-odd Higgs boson, A^0 will confirm extended versions of the Higgs sector directly. At LHC, search of these extra Higgs bosons is also one of the most important tasks. In addition, considerable precision measurement of high energy phenomena may be possible at future linear colliders (LC's) such as JLC, NLC and TESLA[1].

In this paper, we discuss the charged-Higgs-boson production process associated with a W boson at LC's, $e^+e^- \rightarrow H^\pm W^\mp$, in the two-Higgs-Doublet Model (2HDM) including the Minimal Supersymmetric Standard Model (MSSM) with super-heavy super-partner particles. By neglecting the electron mass the process disappears at tree level because of no tree $H^\pm W^\mp V$ couplings ($V = \gamma$ and Z^0) in these models. Since these couplings occur at one-loop level[2, 3, 4], the process $e^+e^- \rightarrow H^\pm W^\mp$ is induced at this level. At LC's, one of the main processes for charged Higgs search is the H^\pm -pair production[5], whose cross section may be large enough to be detected if H^\pm is much lighter than the threshold $\sqrt{s}/2$. The process rapidly reduces for heavier H^\pm even if the mass is below the threshold. In this case $e^+e^- \rightarrow H^\pm W^\mp$ becomes important as a complementary process if its cross section can be large enough to be detected. Our question here is how much this loop-induced process can grow in the non-SUSY 2HDM as well as in the MSSM.

Magnitude of the cross section for $e^+e^- \rightarrow H^\pm W^\mp$ directly shows dynamics of particles in the loop because there is no tree-level contribution. We here consider one-loop contributions of quarks, gauge bosons and Higgs bosons. In particular, the top-bottom (t - b) loop effects are expected to be sizable, because the Yukawa-coupling constants are proportional to quark masses so that the decoupling theorem by Appelquist and Carazzone[6] is not applied to this case. The naive power-counting argument shows that quadratic quark-mass terms appear in the amplitude with a longitudinally polarized W boson. Therefore the t - b loops can greatly contribute to the cross section depending on $\tan \beta$. In the non-SUSY 2HDM, the Higgs-loop contributions can also be large when the Higgs self-coupling constants are proportional to the Higgs boson masses. Effects of the heavy Higgs bosons in the loop then do not decouple in the large mass limit. Instead, the quadratic mass terms of these Higgs bosons can appear in the amplitude[4, 7, 8], so that larger Higgs-loop effects

are expected for heavier Higgs bosons in the loop. In contrast, if masses of the extra Higgs bosons are determined mainly by an independent scale of the vacuum expectation value (~ 246 GeV), the Higgs-loop contributions tend to decouple for large extra-Higgs-boson masses. The MSSM Higgs sector corresponds to this case, so its loop-effects cannot be so large. The main purpose of this paper is to confirm above discussion analytically and numerically and to see the possible enhancement of the cross section by these non-decoupling effects under the requirement for validity of perturbation theory[9, 10, 11, 7]. The information from available experimental data such as the ρ parameter constraint[12] and the $b \rightarrow s\gamma$ results[13, 14] are also taken into account.

We find that the cross section can be quite large for small $\tan\beta$ ($\ll \sqrt{m_t/m_b}$) by the t - b loop effects. In addition, in the non-SUSY 2HDM, the cross section can grow to some extent by the Higgs non-decoupling effects for moderate values of $\tan\beta$. For larger $\tan\beta$ ($\gg \sqrt{m_t/m_b}$) such enhancement by the Higgs-loop effects is strongly bounded by the condition for the perturbation, and the cross section becomes smaller.

In Sec 2, the 2HDM is reviewed briefly to fix our notation. The calculation of the cross section is explained in Sec 3. After some analytic discussion on the amplitude in Sec 4, we present our numerical results in Sec 5. Conclusion is given in Sec 6. Details of the analytic results of the calculation are shown in Appendix.

2 The 2HDM

The 2HDM with a softly-broken discrete symmetry under the transformation $\Phi_1 \rightarrow \Phi_1$, $\Phi_2 \rightarrow -\Phi_2$ is assumed. The Higgs sector is given by

$$\begin{aligned} \mathcal{L}_{\text{THDM}}^{\text{int}} = & \mu_1^2 |\Phi_1|^2 + \mu_2^2 |\Phi_2|^2 + \left\{ \mu_3^2 (\Phi_1^\dagger \Phi_2) + \text{h.c.} \right\} \\ & - \lambda_1 |\Phi_1|^4 - \lambda_2 |\Phi_2|^4 - \lambda_3 |\Phi_1|^2 |\Phi_2|^2 - \lambda_4 (\text{Re}\Phi_1^\dagger \Phi_2)^2 - \lambda_5 (\text{Im}\Phi_1^\dagger \Phi_2)^2. \end{aligned} \quad (1)$$

This potential includes the MSSM Higgs sector as a special case. We here neglect all the CP-violating phases just for simplicity and all the coupling constants and masses are then real in Eq. (1). From the doublets Φ_1 and Φ_2 ($\langle \Phi_i \rangle \equiv v_i/\sqrt{2}$ and $\sqrt{v_1^2 + v_2^2} \sim 246$ GeV), five massive eigenstates as well as three Nambu-Goldstone modes (w^\pm and z^0) are obtained; that is, two CP-even neutral bosons h^0 and H^0 diagonalized by the mixing angle α , one pair of the charged Higgs boson H^\pm , and one CP-odd neutral Higgs boson A^0 , where h^0 is lighter than H^0 . In addition to the four mass parameters m_{h^0} , m_{H^0} , m_{H^\pm} and m_{A^0} , we have two mixing angles α and β ($\tan\beta = v_2/v_1$) and one free dimension-full parameter M corresponding to the soft-breaking mass ($M^2 \equiv \mu_3^2/(\sin\beta \cos\beta)$). Tree-level relations

among the coupling constants and the masses are then given by[4]

$$\lambda_1 = \frac{1}{2v^2 \cos^2 \beta} (\cos^2 \alpha m_{H^0}^2 + \sin^2 \alpha m_{h^0}^2 - \sin^2 \beta M^2), \quad (2)$$

$$\lambda_2 = \frac{1}{2v^2 \sin^2 \beta} (\sin^2 \alpha m_{H^0}^2 + \cos^2 \alpha m_{h^0}^2 - \cos^2 \beta M^2), \quad (3)$$

$$\lambda_3 = \frac{\sin 2\alpha}{v^2 \sin 2\beta} (m_{H^0}^2 - m_{h^0}^2) + \frac{2m_{H^\pm}^2}{v^2} - \frac{1}{v^2} M^2, \quad (4)$$

$$\lambda_4 = -\frac{2m_{H^\pm}^2}{v^2} + \frac{2}{v^2} M^2, \quad (5)$$

$$\lambda_5 = \frac{2}{v^2} (m_{A^0}^2 - m_{H^\pm}^2). \quad (6)$$

As for the Yukawa interaction, two kinds of couplings are possible in our model: we call them Model I and Model II according to Ref. [15]. The Yukawa interaction with respect to the charged-Higgs boson is expressed by

$$\mathcal{L}_{Htb} = \bar{b} \left\{ \frac{y_b}{2} \tan \beta (1 - \gamma_5) + \frac{y_t}{2} \cot \beta (1 + \gamma_5) \right\} t H^- + \text{h.c.}, \quad (7)$$

where

$$y_b = \frac{\sqrt{2}m_b}{v} \cot \beta, \quad y_t = \frac{\sqrt{2}m_t}{v} \cot \beta, \quad (\text{Model I}), \quad (8)$$

$$\text{or} \quad y_b = \frac{\sqrt{2}m_b}{v} \tan \beta, \quad y_t = \frac{\sqrt{2}m_t}{v} \cot \beta, \quad (\text{Model II}). \quad (9)$$

Here Model II corresponds to the MSSM Yukawa-interaction.

3 The calculation for $e^+e^- \rightarrow H^-W^+$

We consider the process $e^-(\tau, k) + e^+(-\tau, \bar{k}) \rightarrow H^-(p) + W^+(\bar{p}, \bar{\lambda})$, where $\tau = \pm 1$ and $\bar{\lambda} = 0, \pm 1$ are helicities of the electron and the W^+ boson; k and \bar{k} are incoming momenta of the electron and the positron, while p and \bar{p} are outgoing momenta of H^- and W^+ , respectively. The helicity amplitude may be written by

$$\mathcal{M}(k, \bar{k}, \tau; p, \bar{p}, \bar{\lambda}) = \sum_{i=1}^3 F_{i,\tau}(s, t) K_{i,\tau}(k, \bar{k}, \tau; p, \bar{p}, \bar{\lambda}), \quad (10)$$

where the form factors $F_{i,\tau}(s, t)$ include all the dynamics that depends on the model. The kinematical factors are expressed by

$$K_{i,\tau}(k, \bar{k}, \tau; p, \bar{p}, \bar{\lambda}) = j_\mu(k, \bar{k}, \tau) T_i^{\mu\beta} \epsilon_\beta(\bar{p}, \bar{\lambda})^*, \quad (11)$$

where $j_\mu(k, \bar{k}, \tau)$ is the electron current and $\epsilon_\beta(\bar{p}, \bar{\lambda})^*$ is the polarization vector of the W boson. The basis tensors $T_i^{\mu\beta}$ are defined by

$$T_1^{\mu\beta} = g^{\mu\beta}, \quad (12)$$

$$T_2^{\mu\beta} = \frac{1}{m_W^2} P^\mu P^\beta, \quad (13)$$

$$T_3^{\mu\beta} = \frac{i}{m_W^2} \epsilon^{\mu\beta\rho\sigma} P_\rho q_\sigma, \quad (14)$$

where $P^\mu \equiv p^\mu - \bar{p}^\mu$, $q^\mu \equiv p^\mu + \bar{p}^\mu = k^\mu + \bar{k}^\mu$ and $\epsilon^{0123} = -1$. In Table 1, the explicit expressions for each $K_{i,\tau}$ in the center-of-mass frame are listed by using β_{HW} and the scattering angle Θ

$$\beta_{HW} = \sqrt{1 - \frac{2(m_W^2 + m_{H^\pm}^2)}{s} + \frac{(m_W^2 - m_{H^\pm}^2)^2}{s^2}}, \quad (15)$$

$$\cos \Theta = \frac{2t + s - m_{H^\pm}^2 - m_W^2}{s\beta_{HW}}, \quad (16)$$

where s and t are the Mandelstam variables ($s = (k + \bar{k})^2 = (p + \bar{p})^2$, $t = (k - p)^2 = (\bar{k} - \bar{p})^2$). The total cross section is calculated according to the formula

$$\sigma(s) = \frac{1}{16\pi} \frac{1}{s^2} \int_{t_{\min}}^{t_{\max}} \frac{1}{2} \sum_\tau \sum_{\bar{\lambda}} |\mathcal{M}(k, \bar{k}, \tau; p, \bar{p}, \bar{\lambda})|^2 dt, \quad (17)$$

where t_{\max} and t_{\min} are defined by

$$t_{\max} = \frac{1}{2}(m_{H^\pm}^2 + m_W^2 - s + s\beta_{HW}), \quad (18)$$

$$t_{\min} = \frac{1}{2}(m_{H^\pm}^2 + m_W^2 - s - s\beta_{HW}). \quad (19)$$

Our formalism here is consistent with that for $e^-e^+ \rightarrow \chi^-W^+$ (χ^- : the charged Goldstone boson) in Ref. [16] in the limit $m_{H^\pm}^2 \rightarrow m_\chi^2$ and also with that for $e^-e^+ \rightarrow H^0\gamma$ in Ref [17].

In calculation, the form factors $F_{i,\tau}(s, t)$ may be decomposed according to each type of Feynman diagrams (Fig. 1) as

$$F_{i,\tau}(s, t) = F_{i,\tau}^\gamma(s) + F_{i,\tau}^Z(s) + F_{i,\tau}^t(t) + F_{i,\tau}^{Box}(s, t) + \delta F_{i,\tau}(s, t), \quad (20)$$

where $F_{i,\tau}^V$ ($V = \gamma$ and Z) are the contribution from the one-loop induced HWV vertices (Fig. 1(a)). These HWV vertices are defined as $igm_W V_{\mu\nu}^{HWV}$ (Fig. 2), in which $V_{\mu\nu}$ may be expressed by[2, 4]

$$\begin{aligned} V_{\mu\nu}^{HWV}(m_{H^\pm}^2, p_W^2, p_V^2) &= F^{HWV}(m_{H^\pm}^2, p_W^2, p_V^2)g_{\mu\nu} + G^{HWV}(m_{H^\pm}^2, p_W^2, p_V^2) \frac{p_{V\mu} p_{W\nu}}{m_W^2} \\ &+ iH^{HWV}(m_{H^\pm}^2, p_W^2, p_V^2) \frac{p_V^\rho p_W^\sigma}{m_W^2} \epsilon_{\mu\nu\rho\sigma}, \end{aligned} \quad (21)$$

where p_H is the incoming momentum of H^- , and p_V ($V = Z$ or γ) and p_W are outgoing momenta of V and W bosons, respectively. The form factor $F_{i,\tau}^V(s)$ are then expressed by

$$F_{1,\tau}^V(s) = gm_W C_V \frac{1}{s - m_V^2} F^{HWV}(m_W^2, s, m_{H^\pm}^2), \quad (22)$$

$$F_{2,\tau}^V(s) = gm_W C_V \frac{1}{s - m_V^2} \frac{1}{2} G^{HWV}(m_W^2, s, m_{H^\pm}^2), \quad (23)$$

$$F_{3,\tau}^V(s) = gm_W C_V \frac{1}{s - m_V^2} \frac{-1}{2} H^{HWV}(m_W^2, s, m_{H^\pm}^2), \quad (24)$$

where m_V is mass of the neutral gauge bosons (m_Z and $m_\gamma (= 0)$), and C_V are defined by $C_\gamma = eQ_e$ and $C_Z = g_Z(T_e^3 - s_W^2 Q_e)$ ($e = g_{SW} = g_Z s_W c_W$), where $Q_e = -1$, and $T_e^3 = -1/2$ (0) for the electron with the helicity $\tau = -1$ ($+1$). The explicit formulas of the F^{HWV} , G^{HWV} , H^{HWV} are given in Appendix A. 1. The $F_{i,\tau}^t(s, t)$ is the contribution of the t channel diagram with the one-loop H^-W^+ mixing diagrams (Fig. 1(b)) and the box diagram contributions are expressed by $F_{i,\tau}^{Box}$ (Fig. 1(c)). We also show the explicit results for $F_{i,\tau}^t$ and $F_{i,\tau}^{Box}$ in Appendix A. 3 and A. 4, respectively. Each one-loop-diagram contribution to $F_1(s, t)$ except for $F_{1,\tau}^{Box}$ includes the ultraviolet divergence. After summing up the contributions $F_{i,t}^V$, $F_{i,\tau}^t$, and $F_{i,\tau}^{Box}$, the divergence is canceled out because of no tree-level contribution.

Although the amplitude is finite already, by making the renormalization for the WH and wH two point functions the finite counterterm, $\delta F_{i,\tau}$, is introduced to this process[18, 19]². By rewriting the fields w^\pm and H^\pm with shifting $\beta \rightarrow \beta - \delta\beta$ by

$$\begin{aligned} \begin{pmatrix} w^\pm \\ H^\pm \end{pmatrix} &\rightarrow \begin{pmatrix} Z_{w^\pm}^{\frac{1}{2}} & Z_{wH}^{\frac{1}{2}} \\ Z_{Hw}^{\frac{1}{2}} & Z_{H^\pm}^{\frac{1}{2}} \end{pmatrix} \begin{pmatrix} 1 & -\delta\beta \\ \delta\beta & 1 \end{pmatrix} \begin{pmatrix} w^\pm \\ H^\pm \end{pmatrix} \\ &\equiv \begin{pmatrix} 1 + \frac{1}{2}Z_{w^\pm}^{(1)} & a_{wH}^{(1)} \\ a_{Hw}^{(1)} & 1 + \frac{1}{2}Z_{H^\pm}^{(1)} \end{pmatrix} \begin{pmatrix} w^\pm \\ H^\pm \end{pmatrix}, \end{aligned} \quad (25)$$

the relevant counterterms are extracted from the kinematic terms of the Higgs sector as

$$\mathcal{L}^{count.} = i a_{wH}^{(1)} \frac{gv}{2} W_\mu^- \partial^\mu H^+ - a_{wH}^{(1)} \frac{g^2 v}{2} \frac{s_W^2}{c_W} W_\mu Z^\mu H^+ + a_{wH}^{(1)} \frac{g^2 v}{2} s_W W_\mu \gamma^\mu H^+ + \text{h.c.} \quad (26)$$

For the WH mixing we take the renormalization condition

$$\text{Re} \left(\Pi_{WH}^{\text{reno.}}(m_{H^\pm}^2) \right) = \text{Re} \left(\Pi_{WH}(m_{H^\pm}^2) \right) + \Pi_{WH}^{\text{count.}} = 0, \quad (27)$$

where $\Pi_{WH}(p^2)$ is given in Eq. (61) in Appendix. we then obtain

$$a_{wH}^{(1)} = \frac{1}{m_W} \text{Re} \left(\Pi_{WH}(m_{H^\pm}^2) \right), \quad (28)$$

²See also **Note Added**.

so that the counterterms for not only the WH mixing but also the HWV vertices are obtained by using Eq. (26). Next, (25) also produces the wH mixing (w : the charged Goldstone boson). We fix the counterterm so as to satisfy the renormalization condition[19]

$$\text{Re} \left(\Pi_{Hw}^{\text{reno.}}(m_{H^\pm}^2) \right) = \text{Re} \left(\Pi_{Hw}(m_{H^\pm}^2) \right) + \Pi_{Hw}^{\text{count.}} = 0. \quad (29)$$

The finite counterterms for the form factors, $\delta F_{i,\tau}$ in Eq. (20), are then obtained as we show in Appendix A.5.

4 Non-decoupling mass effects

Here we present some analytic discussion on the amplitudes to find cases in which the cross section becomes large for a given \sqrt{s} in the non-SUSY 2HDM.

Let us consider the quark-loop contributions to the amplitudes first. They do not decouple in the heavy quark limit because the decoupling theorem[6] does not work for the Yukawa interactions in which the couplings are proportional to the squared masses. Hence larger one-loop effects take place for heavier quark masses³. In the helicity amplitude with a longitudinally polarized W boson, powerlike top- or bottom-quark mass contributions appear by the factor of $m_t^2 \cot \beta$ or $m_b^2 \tan \beta$ in Model II. The linear appearance of $\cot \beta$ or $\tan \beta$ in each factor comes from the fact that one tbH^\pm Yukawa coupling is included in each t - b loop diagram⁴. Each factor becomes large for small $\tan \beta$ ($\ll \sqrt{m_t/m_b}$) or for large $\tan \beta$ ($\gg \sqrt{m_t/m_b}$), respectively. In our analysis, we take into account theoretical lower and upper bounds of $\tan \beta$ putting a criterion for the upper limit of the top-Yukawa coupling y_t ($\propto m_t/\sin \beta$) and the bottom-Yukawa coupling y_b ($\propto m_b/\cos \beta$) by the requirement for validity of perturbation theory. Under the same criterion for both top- and bottom-Yukawa coupling constants, the factor $m_t^2 \cot \beta$ at the lowest $\tan \beta$ value is by m_t/m_b greater than the factor $m_b^2 \tan \beta$ at the highest $\tan \beta$ value. Therefore the helicity amplitude becomes large especially for small $\tan \beta$ ($\ll \sqrt{m_t/m_b}$) by the t - b loop contributions⁵. In Model I, $\tan \beta$ is just replaced by $\cot \beta$ in the coefficient above, hence this change does not affect on above discussion. Therefore in both Model I and II, we expect to have sizable cross sections for small $\tan \beta$ values.

Next we discuss the Higgs-loop contributions. The non-decoupling effects of the heavy Higgs bosons appear only when the Higgs sector has a special property: the Higgs mass

³We here call them as the non-decoupling effects.

⁴The tbH^- coupling gives $m_t \cot \beta$ and $m_b \tan \beta$, and the other m_t and m_b comes from the tbW_L^+ coupling (W_L represent the longitudinal W boson). By the chirality argument other combinations such as $m_t m_b \cot \beta$ and $m_t m_b \tan \beta$ disappear.

⁵ Similar top-bottom quark effects are observed in the cross section of $e^+e^- \rightarrow A^0V$ ($V = \gamma, Z^0$)[20].

squared are expressed like $\sim \lambda_i v^2$, where λ_i is a combination of the Higgs self-coupling constants. This corresponds to $M \ll v$ in our notation[4, 7], where M is the scale of the soft breaking of the discrete symmetry. In this case, similarly to the Yukawa interaction, the terms of $\mathcal{O}(m_{H_i^0}^2/v^2)$ appear in the helicity amplitude with a longitudinally polarized W boson, where H_i^0 represent heavy neutral Higgs bosons in the loop. Therefore, in the non-SUSY 2HDM with the small soft-breaking mass M , these mass effects of heavy Higgs bosons may enhance the amplitude in addition to the t - b loop effects. Clearly, this situation is quite different from the MSSM like Higgs sector, where large masses of the extra Higgs bosons are possible only by taking large M ($\gg \lambda_i v^2 = \mathcal{O}(g^2 v^2)$)⁶.

In order to see the leading non-decoupling effects (the quadratic-mass terms in the large mass limit for particles in the loop) analytically, let us consider the amplitude with a longitudinally polarized W boson in one limiting case. They are extracted from the full expression of the amplitude by taking masses of h^0 , H^0 and A^0 much larger than m_W and m_{H^\pm} with setting $M = 0$ ⁷;

$$\begin{aligned}
& \mathcal{M}(k, \bar{k}, \tau; p, \bar{p}, \bar{\lambda} = 0) \\
&= \sin \Theta \frac{g^2}{c_W^2} \frac{T_e^3}{16\pi^2 v^2} \left[\frac{3}{2} \left\{ \frac{m_{H^0}^2 m_{A^0}^2}{m_{H^0}^2 - m_{A^0}^2} \ln \frac{m_{H^0}^2}{m_{A^0}^2} - \frac{m_{h^0}^2 m_{A^0}^2}{m_{h^0}^2 - m_{A^0}^2} \ln \frac{m_{h^0}^2}{m_{A^0}^2} \right\} J(\alpha, \beta) \right. \\
&\quad - \left. \left\{ \frac{c_{2W}}{2} m_{H^0}^2 + \frac{3}{4} \frac{m_{H^0}^2 m_{A^0}^2}{m_{H^0}^2 - m_{A^0}^2} \ln \frac{m_{H^0}^2}{m_{A^0}^2} \right\} K(\alpha, \beta) \right. \\
&\quad - \left. \left\{ \frac{c_{2W}}{2} m_{h^0}^2 + \frac{3}{4} \frac{m_{h^0}^2 m_{A^0}^2}{m_{h^0}^2 - m_{A^0}^2} \ln \frac{m_{h^0}^2}{m_{A^0}^2} \right\} L(\alpha, \beta) - \frac{N_c}{2} m_t^2 \cot \beta \right] \\
&+ \sin \Theta \frac{g^2 s_W^2 Q_e}{16\pi^2 v^2} \left[\frac{3}{2} \left\{ \frac{m_{H^0}^2 m_{A^0}^2}{m_{H^0}^2 - m_{A^0}^2} \ln \frac{m_{H^0}^2}{m_{A^0}^2} - \frac{m_{h^0}^2 m_{A^0}^2}{m_{h^0}^2 - m_{A^0}^2} \ln \frac{m_{h^0}^2}{m_{A^0}^2} \right\} J(\alpha, \beta) \right. \\
&\quad - \left. \left\{ \frac{1}{2c_W^2} m_{H^0}^2 - \frac{3}{4} \frac{m_{H^0}^2 m_{A^0}^2}{m_{H^0}^2 - m_{A^0}^2} \ln \frac{m_{H^0}^2}{m_{A^0}^2} \right\} K(\alpha, \beta) \right. \\
&\quad - \left. \left\{ \frac{1}{2c_W^2} m_{h^0}^2 - \frac{3}{4} \frac{m_{h^0}^2 m_{A^0}^2}{m_{h^0}^2 - m_{A^0}^2} \ln \frac{m_{h^0}^2}{m_{A^0}^2} \right\} L(\alpha, \beta) + \frac{N_c}{2c_W^2} m_t^2 \cot \beta \right] + \mathcal{O} \left(\frac{s}{m_{H_i^0}^2} \right), \quad (30)
\end{aligned}$$

where H_i^0 represents h^0 , H^0 and A^0 , and

$$J(\alpha, \beta) = \sin(\alpha - \beta) \cos(\alpha - \beta), \quad (31)$$

$$K(\alpha, \beta) = \sin^2 \alpha \cot \beta - \cos^2 \alpha \tan \beta, \quad (32)$$

$$L(\alpha, \beta) = \cos^2 \alpha \cot \beta - \sin^2 \alpha \tan \beta. \quad (33)$$

From the expression (30), we expect that the amplitude can become large by the non-decoupling effects of the heavy Higgs bosons as well as those of the top-quark. The Higgs effects grow for the large or small $\tan \beta$: see (31)-(33).

⁶In the MSSM, m_A corresponds to M .

⁷This expression is for the $\delta F_{i,\tau} = 0$ case.

The non-SUSY 2HDM receives rather strong theoretical constraints. First from the requirement for validity of perturbation theory, all the Higgs-self coupling and Yukawa coupling constants should not be so large[9, 10, 11]. We here set a rather conservative criterion corresponding to Ref. [7]: that is, for the Yukawa couplings

$$y_b^2, y_t^2 < 4\pi, \quad (34)$$

and for the Higgs self-coupling constants

$$|\lambda_1|, |\lambda_2|, |\lambda_3|, \frac{1}{4}|\lambda_4 \pm \lambda_5| < 4\pi. \quad (35)$$

These conditions give constraints on the combinations among masses, mixing angles and the soft-breaking mass. For example, from the condition for λ_1 , we obtain by using (2)

$$(m_{H^0}^2 - M^2) \tan^2 \beta \lesssim 8\pi v^2, \quad (36)$$

for the case of $\alpha = \beta - \pi/2$ and $m_{H^0}^2 \gg m_{h^0}^2$. This means that it is difficult to take large m_{H^0} and large $\tan \beta$ simultaneously with $M^2 \sim 0$. We include all these constraints in our numerical analysis.

Finally the 2HDM is constrained from the precision experimental data[12], especially those for the ρ parameter: the additional contribution of the 2HDM Higgs sector should be small. We here employ the same condition as in Ref. [7]; $\Delta\rho_{2\text{HDM}} = -0.0020 - 0.00049 \frac{m_t - 175\text{GeV}}{5\text{GeV}} \pm 0.0027$. In order to satisfy this there are mainly two kinds of possibility for the parameter choice. A) The Higgs sector is custodial $SU(2)_V$ symmetric ($m_{H^\pm}^2 \sim m_{A^0}^2$). B) The Higgs sector is not custodial $SU(2)_V$ symmetric but there are some relations among parameters to keep a small $\Delta\rho_{2\text{HDM}}$: $m_{H^\pm}^2 \sim m_{H^0}^2$ or $m_{H^\pm}^2 \sim m_{h^0}^2$ with $\alpha \sim \beta - \pi/2$ or $\alpha \sim \beta$, respectively[15]. Also, recent study for the $b \rightarrow s\gamma$ results[13] gives the constraint on the charged Higgs boson mass ($m_{H^\pm} \gtrsim 160$ GeV)[14].

By taking into account all the theoretical and experimental constraints above, the best choice for the maximal Higgs contributions to the cross section is to take the case B) and then to choose m_{A^0} and $\tan \beta$ as large as possible under the conditions (34) and (35).

5 Numerical Evaluation

We here show our numerical results. According to the above analytic discussion, the 7 free parameters of the Higgs sector in the non-SUSY 2HDM ($m_{h^0}^2, m_{H^0}^2, m_{H^\pm}^2, m_{A^0}^2, \alpha, \beta$ and M) are chosen in the following way. To obtain larger Higgs contributions, we take the choice B) in the last section. Since $m_{h^0} < m_{H^0}$, it is better to set $\alpha = \beta - \pi/2$ (or $\alpha = 0$) for larger cross section for $\tan \beta > 1$ ($K(\alpha, \beta) > 1$) (See (32)). If we choose $\alpha = \beta$ (or $\alpha = \pi/2$), then such enhancement takes place for small $\tan \beta$ ($L(\alpha, \beta) \sim 1$). Any

other choice of α leads to smaller cross sections. As for the quark loops, although we here adopt Model II for the Yukawa couplings in actual calculation in the 2HDM, it is clear that there is no difference between Model I and II for the cross section except for the large $\tan\beta$ regime. If we assume the MSSM Higgs sector, there are two free parameters m_{H^\pm} and $\tan\beta$, and all the other parameters are related to these two parameters[15]. As for the quark masses we here fix them as $m_t = 175$ GeV and $m_b = 5$ GeV.

To begin with, we show the total cross section for $m_{H^\pm} = 200$ GeV at $\sqrt{s} = 500$ GeV as a function of $\tan\beta$ (Fig. 3). The region of $\tan\beta$ is $0.28 < \tan\beta < 123$ taking into account the condition (34)⁸, while we switch off the condition (35) in Fig. 3 (and in Fig. 4) just to concentrate on showing the behavior of the non-decoupling effects more clearly. The results in which both the conditions (34) and (35) are included will be shown soon later in Figs. 5 and 6. In Fig. 3, the real curves represent the total cross sections in the non-SUSY 2HDM for each value of m_{A^0} . The other parameters are taken as $m_{h^0} = 120$ GeV, $m_{H^0} = 210$ GeV, $\alpha = \beta - \pi/2$ and $M = 0$. The dotted curve represents the cross section in the MSSM with super-heavy super-partner particles. For small $\tan\beta$ ($\ll \sqrt{m_t/m_b}$), as we discussed in the last section, the cross section is enhanced by the t - b loop contributions both in the MSSM and in the non-SUSY 2HDM. On the other hand, for large $\tan\beta$ ($\gg \sqrt{m_t/m_b}$), the MSSM cross section reduces rapidly, while the Higgs non-decoupling effects enlarge the non-SUSY 2HDM cross section. For larger m_{A^0} , larger cross sections are observed. Our result in the MSSM here is consistent with that in Ref. [24].

Fig. 4 shows the \sqrt{s} dependence of the total cross section in the non-SUSY 2HDM at $m_{H^\pm} = 200$ GeV for various $\tan\beta$, other parameters are chosen as $m_{h^0} = 120$ GeV, $m_{H^0} = 210$ GeV, $m_{A^0} = 1200$ GeV and $\alpha = \beta - \pi/2$ and $M = 0$. The condition (35) is switched off in this figure too.

The enhancement of the cross section essentially depends on the size of the $H^\pm tb$ and $H^\pm H^\mp H^0$ coupling constants. By taking these couplings as large as possible under the conditions (34) and (35) and also under the experimental constraints mentioned before, we obtain upper bounds of the cross section in the non-SUSY 2HDM for each value of m_{H^\pm} and $\tan\beta$. The situation is described in Fig. 5. The dotted curve represents the cross section with $M = 0$ at $\sqrt{s} = 500$ GeV for $m_{H^\pm} = 200$ GeV at $\alpha = \beta - \pi/2$, and all the other free parameters in the Higgs sector are chosen in order to obtain maximum Higgs non-decoupling effects under all the conditions⁹. For $\tan\beta \gtrsim 5.9$, the condition (36) obtained from (35) cannot be satisfied any more if we keep $M = 0$: larger value of $\tan\beta$ is allowed only by introducing nonzero soft-breaking mass M . This leads to the smaller cross section because the non-decoupling property of the Higgs sector is weakened

⁸ As for the constraint for $\tan\beta$ in the MSSM, see Refs. [21, 22, 23].

⁹The other choice of α leads to less Higgs effects for $\tan\beta > 1$ in this case.

by non-zero M : see the discussion in Sec. 4. Therefore the upper bounds are obtained as the solid curve. The cross section rapidly reduces for $\tan\beta \gtrsim 5.9$. Although the quark-loop contributions (the bottom mass effects) enhance the cross section for $\tan\beta \gtrsim 40$, the magnitude is still much less than that for small $\tan\beta$.

In Fig. 6 we show such general bounds of the cross section as a function of $\tan\beta$ at $\sqrt{s} = 500$ GeV for $m_{H^\pm} = 160, 200, 240, 280, 320$ and 360 GeV. All the other free parameters are chosen as the same way in Fig. 5. Each peak of the cross section in the moderate $\tan\beta$ value is the point where the largest Higgs non-decoupling effects with $M = 0$ appear.

6 Discussion and Conclusion

We have discussed the H^\pm production process *via* $e^+e^- \rightarrow H^\pm W^\mp$ in the non-SUSY 2HDM as well as in the MSSM.

In the non-SUSY 2HDM, the large cross section is possible for small $\tan\beta$ by the t - b loop contributions (quadratic top-mass effects). At $\tan\beta = 0.3$, for $m_{H^\pm} = 200$ GeV, the cross section can be as large as 8 fb at $\sqrt{s} = 500$ GeV and maximally it reaches to over 40 fb at $\sqrt{s} \sim 390$ GeV. For larger $\tan\beta$, these top-mass effects decrease until $\tan\beta \sim m_t/m_b = 35$. In Model II, the quadratic bottom-mass effects enhance the cross section for $\tan\beta \gtrsim m_t/m_b$, but the magnitude is not so large: at $\sqrt{s} = 500$ GeV it is at most a few times 10^{-2} fb even for $\tan\beta \sim 100$. If Model I is assumed, this small enhancement for $\tan\beta > m_t/m_b$ disappears, but all the results for smaller $\tan\beta$ are almost same as those in Model II. In addition to the quark-loop effects, the Higgs non-decoupling effects contribute to the cross section by a few times 0.1 fb for moderate values of $\tan\beta$. Such Higgs effects are strongly bounded for larger $\tan\beta$ ($\gtrsim \sqrt{m_t/m_b}$) by the requirement for validity of perturbation theory.

In the MSSM with heavy super-partner particles, the Higgs-loop effects are very small and only the t - b loops contribute to the cross section. For $m_{H^\pm} = 200$ GeV, the cross section at $\tan\beta = 2$ amounts to a few times 0.1 fb at $\sqrt{s} = 500$ GeV, and maximally it reaches to over 1 fb at $\sqrt{s} \sim 390$ GeV. The cross section rapidly reduces for larger $\tan\beta$. We here have not discussed the one-loop contributions of the super-partner particles in the MSSM explicitly, which will be discussed in our future paper.

We give some comments on our analysis. First, our results have been tested in the high-energy limit by using the equivalence theorem[25] at one-loop level[26]. We evaluated $e^-e^+ \rightarrow H^-w^+$ (w^+ : the charged Goldstone boson) and confirmed that the cross section was coincident with our prediction for the $H^-W_L^+$ production in the high-energy limit. Second, although the process is one-loop induced and so the ultraviolet divergences have

canceled among the diagrams, we have include the finite renormalization effects of the WH mixing and the wH mixing by putting the renormalization conditions on the mass shell of H^\pm . The effects have turned out to give a few % (at most about 5%) of corrections to the one-loop-induced cross sections in which the finite renormalization effects ($\delta F_{i,\tau}$) are not included.

Finally we comment on detectability of the signal events for the case of $m_{H^\pm} > m_t + m_b$. The H^\pm decays into a tb pair and the signal process is $e^+e^- \rightarrow H^\pm W^\mp \rightarrow t\bar{b}W^- + \bar{t}bW^+$. The main background process may be $e^+e^- \rightarrow t\bar{t} \rightarrow t\bar{b}W^- + \bar{t}bW^+$. The cross section of $e^+e^- \rightarrow t\bar{t}$ amounts to about 0.57 pb for $\sqrt{s} = 500$ GeV: the signal/background ratio is at most around 1 %. It may be, however, expected that the signal can be comfortably seen if the signal cross section is 10fb, by attaining a background reduction in Ref. [27] by the following method: 1) cut around reconstructed bW masses which can come from bW decay at 175GeV, 2) find a peak in reconstructed m_{H^\pm} and 3) confirm the presence of H^\pm according to the method in Ref. [28]. For smaller signal cross sections of the order of 0.1fb, details of the background analysis are needed to see the detectability.

Note added:

After this work was finished, another paper (Ref. [29]) appeared in which the same subject was studied.

Acknowledgments

The author would like to thank W. Hollik for useful discussion, K. Odagiri for valuable discussion about the backgrounds and the detectability at LC, Y. Okada for useful information about the constraint on $\tan\beta$. This work was supported, in part, by the Alexander von Humboldt Foundation.

A Analytic results

In the formulas here, we use the integral functions introduced by Passarino and Vertman[30]. The notation for the tensor coefficients here is based on Ref. [16]. We here write $A(m_f)$ as $A[f]$, $B_{ij}(p_H^2; m_{f_1}, m_{f_2})$ as $B_{ij}[f_1, f_2]$, $C_{ij}(p_H^2, p_W^2, p_V^2; m_{f_1}, m_{f_2}, m_{f_3})$ as $C_{ij}[f_1, f_2, f_3]$, where f_i are the fields with mass m_{f_i} . For the quark diagrams, we define abbreviation $C_{ij}(tbb) = C_{ij}(p_H^2, p_W^2, p_V^2; m_t, m_b, m_b)$ and $C_{ij}(ttb) = C_{ij}(p_H^2, p_V^2, p_W^2; m_t, m_t, m_b)$. The expression is in the 't Hooft-Feynman gauge. Also $J(\alpha, \beta)$, $K(\alpha, \beta)$ and $L(\alpha, \beta)$ in Eqs. (31) - (33) are written as $J_{\alpha\beta}$, $K_{\alpha\beta}$ and $L_{\alpha\beta}$, and we also write

$$\tilde{K}_{\alpha\beta} = \left\{ K_{\alpha\beta}(m_{H^0}^2 - M^2) - J_{\alpha\beta}(2m_{H^\pm}^2 - m_{H^0}^2) \right\}, \quad (37)$$

$$\tilde{L}_{\alpha\beta} = \left\{ L_{\alpha\beta}(m_{H^0}^2 - M^2) + J_{\alpha\beta}(2m_{H^\pm}^2 - m_{h^0}^2) \right\}, \quad (38)$$

respectively, for brevity. The momentum squared of the H^+ is set on mass-shell, $p_H^2 = m_{H^\pm}^2$.

A.1 Form factors of the $H^+W^-V^0$ ($V^0 = Z^0, \gamma$) Vertices

We write each contribution to the unrenormalized $H^\pm W^\mp V^0$ form factors X^{HWV} , ($X = F, G$ and H) as $X^{HWV} = X^{HWV(a)} + X^{HWV(b)} + X^{HWV(c)}$ corresponding to Figs. 7(a), 7(b) and 7(c). $X^{HWV(a)}$ is the contribution of triangle-type diagrams (Fig. 7(a)), $X^{HWV(b)}$ represents that from the two-point function correction shown in Fig. 7(b), and $X^{HWV(c)}$ is tadpole contribution as well as some two-point function corrections written only by the A function (Fig. 7(c)).

A.1.1 The $H^+W^-Z^0$ vertex

The contribution of triangle-type diagrams to F^{HWZ} is calculated as

$$\begin{aligned} F^{HWZ(a)}(m_{H^\pm}^2, p_W^2, p_Z^2) &= \frac{2}{16\pi^2 v^2 c_W} \\ &\times \left[-\tilde{K}_{\alpha\beta} \left\{ C_{24}[H^\pm A^0 H^0] - c_{2W} C_{24}[H^0 H^\pm H^\pm] \right\} - \tilde{L}_{\alpha\beta} \left\{ C_{24}[H^\pm A^0 h^0] - c_{2W} C_{24}[h^0 H^\pm H^\pm] \right\} \right] \\ &+ J_{\alpha\beta} \left\{ (m_{H^\pm}^2 - m_{H^0}^2) C_{24} \left([w^\pm z^0 H^0] - c_{2W} [H^0 w^\pm w^\pm] \right) - (m_{H^\pm}^2 - m_{A^0}^2) C_{24} [w^\pm H^0 A^0] \right. \\ &- m_W^2 C_{24} [W^\pm H^0 A^0] - \frac{c_{2W}}{c_W} m_W^2 C_{24} [H^\pm H^0 Z^0] - m_W^2 \left(4(p_W^2 + p_W \cdot p_Z) C_0 + 2(2p_W + p_Z) \right. \\ &\left. (p_W C_{11} + p_Z C_{12}) + p_W \cdot p_Z C_{23} + (D-1) C_{24} \right) [W^\pm Z^0 H^0] + c_W^2 m_W^2 \left((p_Z^2 - p_W^2) C_0 \right. \\ &- 2p_Z \cdot (p_W C_{11} + p_Z C_{12}) + p_W \cdot p_Z C_{23} + (D-1) C_{24} \left. \right) [H^0 W^\pm W^\pm] - m_Z^2 (m_{H^\pm}^2 - m_{H^0}^2) s_W^2 C_0 [w^\pm Z^0 H^0] \\ &\left. - m_W^2 (m_{H^\pm}^2 - m_{H^0}^2) s_W^2 C_0 [H^0 W^\pm w^\pm] + m_W^2 s_W^2 C_{24} [H^0 w^\pm W^\pm] - (H^0 \rightarrow h^0) \right\} \\ &+ \frac{4N_c}{16\pi^2 v^2 c_W} \left[m_b^2 \tan \beta \left\{ (-s_W^2 Q_b) \left(p_W \cdot (p_W + p_Z) C_{11} + p_Z \cdot (p_W + p_Z) C_{12} + p_W^2 C_{21} + p_Z^2 C_{22} \right. \right. \right. \end{aligned}$$

$$\begin{aligned}
& +2p_W \cdot p_Z C_{23} + DC_{24} (tbb) - (T_b - s_W^2 Q_b) \left(p_W^2 C_{11} + p_Z \cdot p_Z C_{12} + p_W^2 C_{21} + p_Z^2 C_{22} + 2p_W \cdot p_Z C_{23} \right. \\
& + (D - 2)C_{24} (tbb) - (T_t - s_W^2 Q_t) \left(p_Z^2 C_{11} + p_Z \cdot p_Z C_{12} + p_Z^2 C_{21} + p_W^2 C_{22} + 2p_W \cdot p_Z C_{23} \right. \\
& + (D - 2)C_{24} (tbb) + (-s_W^2 Q_t) m_t^2 C_0 (tbb) \left. \right\} + m_t^2 \cot \beta \left\{ -(T_b - s_W^2 Q_b) \left((p_W^2 + p_W \cdot p_Z) C_0 \right. \right. \\
& + (2p_W^2 + p_W \cdot p_Z) C_{11} + (p_Z^2 + 2p_W \cdot p_Z) C_{12} + p_W^2 C_{21} + p_Z^2 C_{22} + 2p_W \cdot p_Z C_{23} + (D - 2)C_{24} \left. \right) (tbb) \\
& + (-s_W^2 Q_b) m_b^2 C_0 (tbb) + (-s_W^2 Q_t) \left(p_Z \cdot (p_W + p_Z) C_{11} + p_W \cdot (p_W + p_Z) C_{12} + p_Z^2 C_{21} + p_W^2 C_{22} \right. \\
& + 2p_W \cdot p_Z C_{23} + DC_{24} (tbb) - (T_t - s_W^2 Q_t) \left((p_Z^2 + p_W \cdot p_Z) C_0 + (2p_Z^2 + p_W \cdot p_Z) C_{11} \right. \\
& \left. \left. + (p_W^2 + 2p_W \cdot p_Z) C_{12} + p_Z^2 C_{21} + p_W^2 C_{22} + 2p_W \cdot p_Z C_{23} + 2C_{24} \right) (tbb) \right]. \tag{39}
\end{aligned}$$

The contribution of the diagrams expressed in terms of the B_i functions is given by

$$\begin{aligned}
F^{HWZ(b)}(m_{H^\pm}^2, p_W^2, p_Z^2) &= \frac{2}{16\pi^2 v^2 c_W} \left[\frac{1}{2} \tilde{K}_{\alpha\beta} \left\{ s_W^2 B_0 [H^0 H^\pm] + \frac{p_Z^2 - p_W^2}{m_{H^\pm}^2 - m_W^2} c_W^2 (B_0 + 2B_1) [H^0 H^\pm] \right. \right. \\
& + \left. \frac{m_{H^0}^2 - m_{H^\pm}^2}{m_{H^\pm}^2 - m_W^2} s_W^2 B_0 [H^0 H^\pm] \right\} + \frac{1}{2} \tilde{L}_{\alpha\beta} \left\{ s_W^2 B_0 [h^0 H^\pm] + \frac{p_Z^2 - p_W^2}{m_{H^\pm}^2 - m_W^2} c_W^2 (B_0 + 2B_1) [h^0 H^\pm] \right. \\
& + \left. \frac{m_{h^0}^2 - m_{H^\pm}^2}{m_{H^\pm}^2 - m_W^2} s_W^2 B_0 [h^0 H^\pm] \right\} + \frac{1}{2} J_{\alpha\beta} \left\{ -(m_{H^\pm}^2 - m_{H^0}^2) s_W^2 B_0 [H^0 w^\pm] + m_W^2 s_W^2 B_0 (p_W^2; W^\pm H^0) \right. \\
& + m_Z^2 s_W^2 B_0 B_0 (p_Z^2; Z^0 H^0) - \frac{1}{2} \frac{m_W^2}{m_{H^\pm}^2 - m_W^2} s_W^2 \left\{ m_{H^\pm}^2 (B_0 - 2B_1 + B_{21}) + DB_{22} \right\} [H^0 W^\pm] \\
& + \frac{1}{2} m_{H^0}^2 \frac{m_{H^0}^2 - m_{H^\pm}^2}{m_{H^\pm}^2 - m_W^2} s_W^2 B_0 [H^0 w^\pm] + m_W^2 \frac{p_Z^2 - p_W^2}{m_{H^\pm}^2 - m_W^2} c_W^2 (B_0 - B_1) [H^0 W^\pm] \\
& + \left. \frac{m_{H^0}^2 - m_{H^\pm}^2}{m_{H^\pm}^2 - m_W^2} (p_Z^2 - p_W^2) c_W^2 (B_0 + 2B_1) [H^0 w^\pm] - (H^0 \rightarrow h^0) \right\} \left. \right] \\
& + \frac{4N_c}{16\pi^2 v^2 c_W} \left[\frac{s_W^2}{m_{H^\pm}^2 - m_W^2} \left\{ (m_b^2 \tan \beta - m_t^2 \cot \beta) \left(m_{H^\pm}^2 (B_1 + B_{21}) + DB_{22} \right) [tb] \right. \right. \\
& \left. \left. - m_t^2 m_b^2 (\tan \beta - \cot \beta) B_0 [tb] \right\} - \frac{c_W^2}{m_{H^\pm}^2 - m_W^2} (p_Z^2 - p_W^2) \left\{ m_b^2 \tan \beta B_1 + m_t^2 \cot \beta (B_1 + B_0) \right\} [tb] \right]. \tag{40}
\end{aligned}$$

The diagrams relevant to the A -function is expressed by

$$F^{HWZ(c)}(m_{H^\pm}^2, p_W^2, p_Z^2) = \frac{1}{16\pi^2 v^2 c_W} \frac{1}{m_{H^\pm}^2 - m_W^2} \left[s_W^2 \left(\tilde{\Pi}_{Hw}^B - T_1 \right) - \left\{ s_W^2 m_W^2 - c_W^2 (p_Z^2 - m_W^2) \right\} T_2 \right], \tag{41}$$

where $\tilde{\Pi}_{Hw}^B$, T_1 and T_2 are given in (57), (58) and (55).

The contribution of the triangle type diagrams to G^{HWZ} and H^{HWZ} are given by

$$\begin{aligned}
G^{HWZ(a)}(m_{H^\pm}^2, p_W^2, p_Z^2) &= \frac{2m_W^2}{16\pi^2 v^2 c_W} \left[-\tilde{K}_{\alpha\beta} (C_{12} + C_{23}) \left\{ [H^\pm A^0 H^0] - c_{2W} [H^0 H^\pm H^\pm] \right\} \right. \\
& - \tilde{L}_{\alpha\beta} (C_{12} + C_{23}) \left\{ [H^\pm A^0 h^0] - c_{2W} [h^0 H^\pm H^\pm] \right\} \\
& + J_{\alpha\beta} \left\{ (m_{H^\pm}^2 - m_{H^0}^2) (C_{12} + C_{23}) [w^\pm z^0 H^0] - (m_{H^\pm}^2 - m_{H^0}^2) c_{2W} (C_{12} + C_{23}) [H^0 w^\pm w^\pm] \right\}
\end{aligned}$$

$$\begin{aligned}
& -(m_{H^\pm}^2 - m_{A^0}^2)(C_{12} + C_{23})[w^\pm H^0 A^0] - m_W^2 (2C_0 + 2C_{11} + C_{12} + C_{23}) [W^\pm H^0 A^0] \\
& - \frac{c_{2W}}{c_W} m_W^2 (-C_{12} + C_{23}) [H^\pm H^0 Z^0] + m_W^2 (2C_0 - 2C_{11} + 5C_{12} + C_{23}) [W^\pm Z^0 H^0] \\
& + c_W^2 m_W^2 (4C_{11} - 3C_{12} - C_{23}) [H^0 W^\pm W^\pm] + m_W^2 s_W^2 (C_{23} - C_{12}) [H^0 w^\pm W^\pm] - (H^0 \rightarrow h^0) \Big\} \\
& + \frac{4N_c m_W^2}{16\pi^2 v^2 c_W} \left[m_b^2 \tan \beta \left\{ (-s_W^2 Q_b)(C_{12} - C_{11})(tbb) + (T_b - s_W^2 Q_b)(2C_{23} + C_{12})(tbb) \right. \right. \\
& + (T_t - s_W^2 Q_t)(C_{12} + 2C_{23})(tbb) \Big\} + m_t^2 \cot \beta \left\{ (T_b - s_W^2 Q_b)(C_0 + C_{11} + 2C_{12} + 2C_{23})(tbb) \right. \\
& \left. \left. - (-s_W^2 Q_t)(C_{11} - C_{12})(tbb) + (T_t - s_W^2 Q_t)(C_0 + C_{11} + 2C_{12} + 2C_{23})(tbb) \right\} \right]. \tag{42}
\end{aligned}$$

$$\begin{aligned}
H^{HWZ(a)}(m_{H^\pm}^2, p_W^2, p_Z^2) &= \frac{4N_c m_W^2}{16\pi^2 v^2 c_W} \left[m_b^2 \tan \beta (-s_W^2 Q_b) \left\{ (C_{12} - C_{11})(tbb) - (T_b - s_W^2 Q_b)C_{12}(tbb) \right. \right. \\
& \left. \left. - (T_t - s_W^2 Q_t)C_{12}(tbb) \right\} + m_t^2 \cot \beta \left\{ -(T_b - s_W^2 Q_b)(C_0 + C_{11})(tbb) - (s_W^2 Q_t)(C_{11} - C_{12})(tbb) \right. \right. \\
& \left. \left. - (T_t - s_W^2 Q_t)(C_0 + C_{11})(tbb) \right\} \right]. \tag{43}
\end{aligned}$$

There is no contribution from the other diagrams to G^{HWZ} and H^{HWZ} ;

$$G^{HWZ(b)} = G^{HWZ(c)} = H^{HWZ(b,c)} = 0. \tag{44}$$

A.1.2 The $H^+W^-\gamma$ vertex

By making the similar decomposition to the HWZ vertex, we obtain contributions of the $H^+W^-\gamma$ vertex to each form factor.

$$\begin{aligned}
F^{HW\gamma(a)}(m_{H^\pm}^2, p_W^2, p_\gamma^2) &= \frac{4s_W}{16\pi^2 v^2} \times \left[\tilde{K}_{\alpha\beta} C_{24} [H^0 H^\pm H^\pm] + \tilde{L}_{\alpha\beta} C_{24} [h^0 H^\pm H^\pm] \right. \\
& + J_{\alpha\beta} \left\{ \frac{m_W^2}{2} \left((p_\gamma^2 - p_W^2)C_0 - 2p_\gamma \cdot (p_W C_{11} + p_\gamma C_{12}) + p_W \cdot p_\gamma C_{23} + (D-1)C_{24} \right) [H^0 W^\pm W^\pm] \right. \\
& + \frac{m_W^2}{2} (m_{H^\pm}^2 - m_{H^0}^2) C_0 [H^0 W^\pm w^\pm] - \frac{m_W^2}{2} C_{24} [H^0 w^\pm W^\pm] - (m_{H^\pm}^2 - m_{H^0}^2) C_{24} [H^0 w^\pm w^\pm] \\
& \left. \left. - (H^0 \rightarrow h^0) \right\} \right] + \frac{4s_W N_c}{16\pi^2 v^2} \left[m_b^2 \tan \beta \left\{ Q_b \left(p_W \cdot (p_W + p_\gamma) C_{11} + p_\gamma \cdot (p_W + p_\gamma) C_{12} + p_W^2 C_{21} + p_\gamma^2 C_{22} \right. \right. \right. \\
& + 2p_W \cdot p_\gamma C_{23} + 4C_{24} \Big) (tbb) - Q_b \left(p_W^2 C_{11} + p_W \cdot p_\gamma C_{12} + p_W^2 C_{21} + p_\gamma^2 C_{22} + 2p_W \cdot p_\gamma C_{23} + 2C_{24} \right) (tbb) \\
& \left. \left. - m_b^2 \tan \beta Q_t \left(p_\gamma^2 C_{11} + p_\gamma \cdot p_Z C_{12} + p_\gamma^2 C_{21} + p_W^2 C_{22} + 2p_W \cdot p_\gamma C_{23} + 2C_{24} \right) (tbb) + m_t^2 Q_t C_0 (tbb) \right\} \right. \\
& + m_t^2 \cot \beta \left\{ -Q_b \left((p_W^2 + p_W \cdot p_\gamma) C_0 + (2p_W^2 + p_W \cdot p_\gamma) C_{11} + (p_\gamma^2 + 2p_W \cdot p_\gamma) C_{12} + p_W^2 C_{21} + p_\gamma^2 C_{22} \right. \right. \\
& + 2p_W \cdot p_\gamma C_{23} + 2C_{24} \Big) (tbb) + m_b^2 Q_b C_0 (tbb) + Q_t \left(p_\gamma \cdot (p_W + p_\gamma) C_{11} + p_W \cdot (p_W + p_\gamma) C_{12} \right. \\
& + p_\gamma^2 C_{21} + p_W^2 C_{22} + 2p_W \cdot p_\gamma C_{23} + 4C_{24} \Big) (tbb) - Q_t \left((p_\gamma^2 + p_W \cdot p_\gamma) C_0 + (2p_\gamma^2 + p_W \cdot p_\gamma) C_{11} \right. \\
& \left. \left. + (p_W^2 + 2p_W \cdot p_\gamma) C_{12} + p_\gamma^2 C_{21} + p_W^2 C_{22} + 2p_W \cdot p_\gamma C_{23} + 2C_{24} \right) (tbb) \right]. \tag{45}
\end{aligned}$$

$$F^{HW\gamma(b)}(m_{H^\pm}^2, p_W^2, p_\gamma^2) = \frac{4s_W}{16\pi^2 v^2} \times \left[-\frac{1}{4} \tilde{K}_{\alpha\beta} \left\{ B_0 [H^0 H^\pm] + \frac{m_{H^0}^2 - m_{H^\pm}^2}{m_{H^\pm}^2 - m_W^2} B_0 [H^0 H^\pm] \right. \right.$$

$$\begin{aligned}
& -\frac{p_\gamma^2 - p_W^2}{m_{H^\pm}^2 - m_W^2} (B_0 + 2B_1)[H^0 H^\pm] \Big\} - \frac{1}{4} \tilde{L}_{\alpha\beta} \left\{ B_0[h^0 H^\pm] + \frac{m_{h^0}^2 - m_{H^\pm}^2}{m_{H^\pm}^2 - m_W^2} B_0[h^0 H^\pm] \right. \\
& - \frac{p_\gamma^2 - p_W^2}{m_{H^\pm}^2 - m_W^2} (B_0 + 2B_1)[h^0 H^\pm] \Big\} + J_{\alpha\beta} \left\{ \frac{1}{4} (m_{H^\pm}^2 - m_{H^0}^2) B_0[H^0 w^\pm] - \frac{m_W^2}{2} B_0(p_W^2; W^\pm H^0) \right. \\
& + \frac{1}{4} \frac{m_W^2}{m_{H^\pm}^2 - m_W^2} \left\{ m_{H^\pm}^2 (B_0 - 2B_1 + B_{21}) + DB_{22} \right\} [H^0 W^\pm] - \frac{m_{H^0}^2}{4} \frac{m_{H^0}^2 - m_{H^\pm}^2}{m_{H^\pm}^2 - m_W^2} B_0[H^0 w^\pm] \\
& + \frac{1}{2} \frac{m_{H^0}^2 - m_{H^\pm}^2}{m_{H^\pm}^2 - m_W^2} (p_\gamma^2 - p_W^2) (B_0 + 2B_1)[H^0 w^\pm] + \frac{m_W^2}{2} \frac{p_\gamma^2 - p_W^2}{m_{H^\pm}^2 - m_W^2} (B_0 - B_1)[H^0 W^\pm] - (H^0 \rightarrow h^0) \Big\} \\
& + \frac{4s_W}{16\pi^2 v^2} \left[-\frac{p_\gamma^2 - p_W^2}{m_{H^\pm}^2 - m_W^2} \left\{ m_b^2 \tan \beta B_1 + m_t^2 \cot \beta (B_1 + B_0) \right\} [tb] \right. \\
& \left. - \frac{1}{m_{H^\pm}^2 - m_W^2} \left\{ (m_b^2 \tan \beta - m_t^2 \cot \beta) (m_{H^\pm}^2 (B_1 + B_{21}) + DB_{22}) + m_t^2 m_b^2 (\tan \beta - \cot \beta) B_0 \right\} [tb] \right]. \quad (46)
\end{aligned}$$

$$F^{HW\gamma(c)}(m_{H^\pm}^2, p_W^2, p_\gamma^2) = -\frac{s_W}{16\pi^2 v^2} \frac{1}{m_{H^\pm}^2 - m_W^2} \left\{ \tilde{\Pi}_{Hw}^B - T_1 + (p_\gamma^2 - p_W^2 + m_W^2) T_2 \right\}. \quad (47)$$

where T_1 and T_2 and $\tilde{\Pi}_{Hw}^B$ are defined in (57), (58) and (55).

$$\begin{aligned}
G^{HW\gamma(a)}(m_{H^\pm}^2, p_W^2, p_\gamma^2) &= \frac{4m_W^2 s_W}{16\pi^2 v^2} \left[\tilde{K}_{\alpha\beta} (C_{12} + C_{23}) [H^0 H^\pm H^\pm] + \tilde{L}_{\alpha\beta} (C_{12} + C_{23}) [h^0 H^\pm H^\pm] \right. \\
& + J_{\alpha\beta} \left\{ \frac{m_W^2}{2} (4C_{11} - 3C_{12} - C_{23}) [H^0 W^\pm W^\pm] + \frac{m_W^2}{2} (C_{12} - C_{23}) [H^0 w^\pm W^\pm] \right. \\
& \left. - (m_{H^\pm}^2 - m_{H^0}^2) (C_{12} + C_{23}) [H^0 w^\pm w^\pm] - (H^0 \rightarrow h^0) \right\} + \frac{4m_W^2 s_W N_c}{16\pi^2 v^2} \left[m_b^2 \tan \beta Q_b (C_{12} - C_{11}) (tbb) \right. \\
& + m_b^2 \tan \beta Q_b (2C_{23} + C_{12}) (tbb) + m_t^2 \cot \beta Q_b (C_0 + C_{11} + 2C_{12} + 2C_{13}) (tbb) + m_t^2 \cot \beta Q_t \\
& \left. \times (C_{12} - C_{11}) (tbb) + m_b^2 \tan \beta Q_t (2C_{23} + C_{12}) (tbb) + m_t^2 \cot \beta Q_t (C_0 + C_{11} + 2C_{12} + 2C_{23}) (tbb) \right] \quad (48)
\end{aligned}$$

$$\begin{aligned}
H^{HW\gamma(a)}(m_{H^\pm}^2, p_W^2, p_\gamma^2) &= \frac{4m_W^2 s_W N_c}{16\pi^2 v^2} \left[m_b^2 \tan \beta Q_b (C_{12} - C_{11}) (tbb) - m_b^2 \tan \beta Q_b C_{12} (tbb) \right. \\
& - m_t^2 \cot \beta Q_b (C_0 + C_{11}) (tbb) + m_t^2 \cot \beta Q_t (C_{11} - C_{12}) (tbb) - m_b^2 \tan \beta Q_t C_{12} (tbb) \\
& \left. - m_t^2 \cot \beta Q_t (C_0 + C_{11}) (tbb) \right]. \quad (49)
\end{aligned}$$

and

$$G^{HW\gamma(b,c)} = H^{HW\gamma(b,c)} = 0. \quad (50)$$

A.2 Tadpole diagrams and the w - H two point function

The tadpole graphs iT_H and iT_h are calculated as

$$T_H = \frac{1}{16\pi^2 v} \left[m_{H^0}^2 \cos(\alpha - \beta) \left(A[w^\pm] + \frac{1}{2} A[z^0] \right) \right]$$

$$\begin{aligned}
& + \left\{ \left(\frac{\cos \alpha \sin^2 \beta}{\cos \beta} - \frac{\sin \alpha \cos^2 \beta}{\sin \beta} \right) m_{H^0}^2 + 2 \cos(\alpha - \beta) m_{H^\pm}^2 + \frac{\sin(\alpha + \beta)}{\sin \beta \cos \beta} M^2 \right\} A[H^\pm] \\
& + \left\{ \left(\frac{\cos \alpha \sin^2 \beta}{\cos \beta} - \frac{\sin \alpha \cos^2 \beta}{\sin \beta} \right) m_{H^0}^2 + 2 \cos(\alpha - \beta) m_{A^0}^2 + \frac{\sin(\alpha + \beta)}{\sin \beta \cos \beta} M^2 \right\} \frac{1}{2} A[A^0] \\
& + \frac{3}{2} \left\{ \left(\frac{\cos^3 \alpha}{\cos \beta} + \frac{\sin^3 \alpha}{\sin \beta} \right) m_{H^0}^2 - \frac{\cos 2\beta}{\cos \beta \sin \beta} \sin(\alpha - \beta) M^2 \right\} A[H^0] \\
& + \left\{ \frac{1}{2} (m_{H^0}^2 + 2m_{h^0}^2) \frac{\sin 2\alpha}{\sin 2\beta} - \frac{M^2}{4 \cos \beta \sin \beta} (-3 \sin 2\alpha + \sin 2\beta) \right\} \cos(\alpha - \beta) A[h^0] \\
& + 8 \cos(\alpha - \beta) \left(m_W^2 A[W^\pm] + \frac{1}{2} m_Z^2 A[Z^0] \right) - 4N_c \left(\frac{\cos \alpha}{\cos \beta} A[b] + \frac{\sin \alpha}{\sin \beta} A[t] \right), \tag{51}
\end{aligned}$$

$$\begin{aligned}
T_h & = \frac{1}{16\pi^2 v} \left[-m_{h^0}^2 \sin(\alpha - \beta) \left(A[w^\pm] + \frac{1}{2} A[z^0] \right) \right. \\
& + \left\{ \left(\frac{\sin \alpha \sin^2 \beta}{\cos \beta} - \frac{\cos \alpha \cos^2 \beta}{\sin \beta} \right) m_{h^0}^2 - 2 \sin(\alpha - \beta) m_{H^\pm}^2 + \frac{\cos(\alpha + \beta)}{\sin \beta \cos \beta} M^2 \right\} A[H^\pm] \\
& + \left\{ \left(\frac{\sin \alpha \sin^2 \beta}{\cos \beta} - \frac{\cos \alpha \cos^2 \beta}{\sin \beta} \right) m_{h^0}^2 - 2 \sin(\alpha - \beta) m_{A^0}^2 + \frac{\cos(\alpha + \beta)}{\sin \beta \cos \beta} M^2 \right\} \frac{1}{2} A[A^0] \\
& - \frac{3}{2} \left\{ \left(\frac{\sin^3 \alpha}{\cos \beta} - \frac{\cos^3 \alpha}{\sin \beta} \right) m_{h^0}^2 + \frac{\cos 2\beta}{\cos \beta \sin \beta} \cos(\alpha - \beta) M^2 \right\} A[h^0] \\
& + \frac{1}{2} \left\{ (2m_{H^0}^2 + m_{h^0}^2) \frac{\sin 2\alpha}{\sin 2\beta} - \frac{M^2}{4 \cos \beta \sin \beta} (3 \sin 2\alpha + \sin 2\beta) \right\} \sin(\alpha - \beta) A[H^0] \\
& \left. - 8 \sin(\alpha - \beta) \left(m_W^2 A[W^\pm] + \frac{1}{2} m_Z^2 A[Z^0] \right) - 4N_c \left(\frac{\sin \alpha}{\cos \beta} A[b] + \frac{\cos \alpha}{\sin \beta} A[t] \right) \right]. \tag{52}
\end{aligned}$$

The w - H two point function is given by

$$\Pi_{wH}(p^2) = \Pi_{wH}^A(p^2) + \Pi_{wH}^B + \Pi_{wH}^C, \tag{53}$$

where Π_{wH}^B is the contribution of the diagrams which include a quartic Higgs-self coupling constants and Π_{wH}^C is the tadpole contributions. The explicit formulas are

$$\begin{aligned}
\Pi_{Hw}^A(m_{H^\pm}^2) & = \frac{1}{16\pi^2 v^2} \left[(m_{H^0}^2 - m_{H^\pm}^2) \tilde{K}_{\alpha\beta} B_0[H^0 H^\pm] + (m_{h^0}^2 - m_{H^\pm}^2) \tilde{L}_{\alpha\beta} B_0[h^0 H^\pm] + J_{\alpha\beta} \left\{ -m_W^2 \right. \right. \\
& \times \left(p^2 (B_0 - 2B_1 + B_{21}) + DB_{22} \right) [H^0 W^\pm] + m_{H^0}^2 (m_{H^0}^2 - m_{H^\pm}^2) B_0[H^0 w^\pm] - (H^0 \rightarrow h^0) \left. \right\} \\
& + \frac{4N_c}{16\pi^2 v^2} \left[(m_b^2 \tan \beta - m_t^2 \cot \beta) \left(m_{H^\pm}^2 (B_1 + B_{21}) + DB_{22} \right) [tb] - m_t^2 m_b^2 (\tan \beta - \cot \beta) B_0[tb] \right], \tag{54}
\end{aligned}$$

$$\begin{aligned}
\Pi_{Hw}^B & = \frac{1}{16\pi^2 v^2} \tilde{\Pi}_{Hw}^B = \frac{1}{16\pi^2 v^2} \left[2(m_{H^0}^2 - m_{h^0}^2) J_{\alpha\beta} \left(A[W^\pm] + \frac{1}{4} A[Z^0] \right) \right. \\
& 2 \left\{ + (K_{\alpha\beta} - J_{\alpha\beta}) m_{H^0}^2 + (L_{\alpha\beta} + J_{\alpha\beta}) m_{h^0}^2 - 2 \cot 2\beta M^2 \right\} \left(A[H^\pm] + \frac{1}{4} A[A^0] \right) \\
& + J_{\alpha\beta} m_{H^\pm}^2 \left(A[h^0] - A[H^0] \right) + \frac{1}{4} \sin 2\beta \left(\frac{\sin^4 \alpha}{\sin^2 \beta} - \frac{\cos^4 \alpha}{\cos^2 \beta} + \frac{\sin 2\alpha \cos 2\alpha}{\sin 2\beta} \right) m_{H^0}^2 A[H^0] \\
& \left. + \frac{1}{4} \sin 2\beta \left(\frac{\cos^4 \alpha}{\sin^2 \beta} - \frac{\sin^4 \alpha}{\cos^2 \beta} + \frac{\sin 2\alpha \cos 2\alpha}{\sin 2\beta} \right) m_{h^0}^2 A[h^0] \right]
\end{aligned}$$

$$\begin{aligned}
& + \frac{1}{4} \sin 2\beta \left(\frac{\sin^2 \alpha \cos^2 \alpha}{\sin^2 \beta} - \frac{\sin^2 \alpha \cos^2 \alpha}{\cos^2 \beta} - \frac{\sin 2\alpha \cos 2\alpha}{\sin 2\beta} \right) \left(m_{h^0}^2 A[H^0] + m_{H^0}^2 A[h^0] \right) \\
& - \frac{M^2}{2} \frac{\cos 2\beta}{\cos \beta \sin \beta} \left(\sin^2(\alpha - \beta) A[H^0] + \cos^2(\alpha - \beta) A[h^0] \right) \Bigg], \tag{55}
\end{aligned}$$

$$\Pi_{Hw}^C = \frac{1}{v} \left(-T_1 + m_{H^\pm}^2 T_2 \right), \tag{56}$$

where

$$T_1 = 16\pi^2 v^2 \{ \sin(\alpha - \beta) T_H + \cos(\alpha - \beta) T_h \}, \tag{57}$$

$$T_2 = 16\pi^2 v^2 \left\{ \frac{1}{m_{H^0}^2} \sin(\alpha - \beta) T_H + \frac{1}{m_{h^0}^2} \cos(\alpha - \beta) T_h \right\}. \tag{58}$$

A.3 The t channel contribution

The contribution of the t -channel diagram (Fig. 1(b)) is only from the $W^+ H^-$ mixing. When we write the $W^\mu H$ two-point function as

$$i\Pi_{WH}^\mu(p) = ip^\mu \Pi_{WH}(p^2), \tag{59}$$

the contribution to the form factor is expressed as

$$F_{i,\tau}^t(t) = \delta_{i,1} \delta_{\tau,-1} \frac{g^2}{2} \frac{1}{m_{H^\pm}^2 - m_W^2} \Pi_{WH}(m_{H^\pm}^2). \tag{60}$$

where

$$\begin{aligned}
\Pi_{WH}(p^2) &= \frac{m_W}{16\pi^2 v^2} \left[\tilde{K}_{\alpha\beta} (2B_1 + B_0) [H^0 H^\pm] + \tilde{L}_{\alpha\beta} (2B_1 + B_0) [h^0 H^\pm] \right. \\
& \quad \left. + J_{\alpha\beta} \left\{ 2m_W^2 (B_0 - B_1) [H^0 W^\pm] + (m_{H^0}^2 - m_{H^\pm}^2) (2B_1 + B_0) [H^0 w^\pm] - (H^0 \rightarrow h^0) \right\} \right. \\
& \quad \left. - 4N_c \left\{ m_b^2 \tan \beta B_1 + m_t^2 \cot \beta (B_1 + B_0) \right\} [tb] - T_2 \right], \tag{61}
\end{aligned}$$

where the tadpole contribution T_2 is given in (58).

A.4 The box-diagram

The contribution from the box diagrams (Fig. 1(c)) is parametrized as

$$F_{i,\tau}^{\text{box}}(s, t) = -\frac{1}{16\pi^2} \frac{g^4}{4} m_W J_{\alpha\beta} \left\{ f_i^{\text{box}}[\nu, W, H^0, W] - f_i^{\text{box}}[\nu, W, h^0, W] \right\} \delta_{\tau,-1}. \tag{62}$$

The functions f_i^{box} are calculated as

$$f_1^{\text{box}}[\nu, W, S, W] = \left\{ 2(t - m_{H^\pm}^2) D_{11} + 2m_{H^\pm}^2 D_{12} + (s - m_{H^\pm}^2 - m_W^2) D_{13} \right.$$

$$\begin{aligned}
& +m_{H^\pm}^2 D_{22} + m_W^2 D_{23} + (t - m_{H^\pm}^2) D_{24} + (-s - t + m_{H^\pm}^2) D_{25} \\
& + (s - m_{H^\pm}^2 - m_W^2) D_{26} + 4D_{27} \} [\nu, W, S, W], \tag{63}
\end{aligned}$$

$$f_2^{\text{box}}[\nu, W, S, W] = m_W^2 D_{13}[\nu, W, S, W], \tag{64}$$

$$f_3^{\text{box}}[\nu, W, S, W] = m_W^2 \left(\frac{1}{2} D_{11} + D_{13} \right) [\nu, W, S, W], \tag{65}$$

where

$$D_{ij}[\nu, W, S, W] = D_{ij}(k^2, p_H^2, p_W^2, \bar{k}^2; 0, m_W, m_S, m_W), \quad (S = h^0, H^0). \tag{66}$$

A.5 Finite renormalization effects

The counterterm in Eq. (20) is obtained in terms of $\text{Re}(\Pi_{HW}(m_{H^\pm}^2))$ and $\text{Re}(\Pi_{Hw}(m_{H^\pm}^2))$. We decompose $\delta F_{i,\tau}$ into three parts as similarly to the one-loop diagram part in Eq. (20),

$$\delta F_{i,\tau}(s, t) = \delta F_{i,\tau}^Z(s) + \delta F_{i,\tau}^\gamma(s) + \delta F_{i,\tau}^t(t). \tag{67}$$

where each part in RHS is written

$$\delta F_{i,\tau}^V(s) = \delta_{i,1} g m_W C_V \frac{1}{s - m_V^2} \delta F^{HWV}(m_W^2, s, m_{H^\pm}^2), \tag{68}$$

$$\delta F_{i,\tau}^t(t) = -\delta_{i,1} \delta_{\tau,-1} \frac{g^2}{2(m_{H^\pm}^2 - m_W^2)} \text{Re}(\Pi_{WH}(m_{H^\pm}^2)). \tag{69}$$

where V represents Z or γ , and $F^{HWV}(m_W^2, m_Z^2)$ and $F_{i,\tau}^t$ are expressed by

$$\begin{aligned}
\delta F^{HWZ}(p_W^2, p_Z^2, m_{H^\pm}^2) &= \frac{1}{c_W} \left(c_W^2 \frac{p_W^2 - p_Z^2}{m_{H^\pm}^2 - m_W^2} - s_W^2 \right) \frac{1}{m_W} \text{Re}(\Pi_{WH}(m_{H^\pm}^2)) \\
&\quad - \frac{1}{c_W} \frac{s_W^2 m_{H^\pm}^2}{m_{H^\pm}^2 - m_W^2} \text{Re}(\Pi_{wH}(m_{H^\pm}^2)), \tag{70}
\end{aligned}$$

$$\begin{aligned}
\delta F^{HW\gamma}(p_W^2, p_\gamma^2, m_{H^\pm}^2) &= s_W \left(1 + \frac{p_W^2 - p_\gamma^2}{m_{H^\pm}^2 - m_W^2} \right) \frac{1}{m_W} \text{Re}(\Pi_{WH}(m_{H^\pm}^2)) \\
&\quad + \frac{s_W}{m_{H^\pm}^2 - m_W^2} \text{Re}(\Pi_{wH}(m_{H^\pm}^2)), \tag{71}
\end{aligned}$$

where $\Pi_{wH}(p^2)$ and $\Pi_{WH}(p^2)$ are given in Eqs. (53) and (61).

References

- [1] *JLC-1*, KEK Report 92-16 (1992); *Physics and Technology of the Next Linear Collider: a Report submitted to Snowmass 1996*, BNL 52-502, FNAL-PUB-96/112, LBNL-PUB-5425, SLAC Report 485, UCRL-ID-124160; TESLA TECHNICAL DESIGN REPORT: Physics and Detector (<http://www.desy.de/~behnke/tdr/Welcome.html>).
- [2] A. Méndez and A. Pomarol, *Nucl. Phys. B* **349** (1991) 369.
- [3] M. Capdequi Peyranère, H.E. Haber and P. Irulegui, *Phys. Rev. D* **44** (1991) 191.
- [4] S. Kanemura, *Phys. Rev. D* **61** (2000) 095001.
- [5] A. Arhrib, M. Capdequi Peyranère and G. Moultaqa, *Phys. Lett. B* **341** (1995) 313; J. Guasch, W. Hollik and A. Kraft, Talk at the Vth workshop in the 2nd ECFA/DESY Study on Physics and Detectors For a Linear Electron-Positron Collider, Obernai (France) 16-19th Oct. 1999 (hep-ph/9911452).
- [6] T. Appelquist and J. Carazzone, *Phys. Rev. D* **11** (1975) 2856.
- [7] S. Kanemura, T. Kasai and Y. Okada, *Phys. Lett. B* **471** (1999) 182.
- [8] P. Ciafaloni and D. Esprin, *Phys. Rev. D* **56** (1997) 1752; S. Kanemura and H-A. Tohyama, *Phys. Rev. D* **57** (1998) 2949.
- [9] H. Hüffel and G. Pocsik, *Z. Phys. C* **8** (1981) 13; J. Maalampi, J. Sirkka and I. Vilja, *Phys. Lett. B* **265** (1991) 371; S. Kanemura, T. Kubota and E. Takasugi, *Phys. Lett. B* **313** (1993) 155.
- [10] H. Komatsu, *Prog. Theor. Phys.* **67** (1982) 1177; R. A. Flores and M. Sher, *Ann. Phys. (NY)* **148** (1983) 295; M. Sher, *Phys. Rep.* **179** (1989) 273; D. Kominis and R.S. Chivukula, *Phys. Lett. B* **304** (1993) 152; S. Nie and M. Sher, *Phys. Lett. B* **449** (1999) 89.
- [11] Y. Grossman, *Nucl. Phys. B* **426** (1994) 355.
- [12] A.K. Grant, *Phys. Rev. D* **51** (1995) 207; P.H. Chankowski, M. Krawczyk and J. Zochowski, *Eur. Phys. J. C* **11** (1999) 661.
- [13] CLEO Collaboration, CLEO CONF 98-17, ICHEP98 1011.
- [14] M. Ciuchini, G. Degrassi, P. Gambini and G.F. Giudice, *Nucl. Phys. B* **527** (1998) 21; P. Ciafaloni, A. Romanino and A. Strumia, *Nucl. Phys. B* **524** (1998) 361;

- F. Borzumati and G. Greub, *Phys. Rev. D* **58** (1998) 074004, *ibid.* **59** (1999) 057501; T.M. Aliev and E.O. Iltan, *Phys. Rev. D* **58** (1998) 095014.
- [15] J.F. Gunion, H.E. Haber, G. Kane and S. Dawson, *The Higgs Hunter's Guide*, (Addison-Wesley, New York, 1990).
- [16] S. Alam, K. Hagiwara, S. Kanemura, R. Szalapski and Y. Umeda, *Nucl. Phys. B* **541** (1999) 50.
- [17] A. Djouadi, V. Driesen, W. Hollik and J. Rosiek, *Nucl. Phys. B* **491** (1997) 68.
- [18] A. Dabelstein, *Nucl. Phys. B* **456** (1995) 25; M. Böhm, W. Hollik and H. Spiesberger, *Fortschr. Phys.* **34** (1986) 11.
- [19] M. Capdequi Peyranère, *Int. Mod. Phys. A* **14** (1999) 429.
- [20] A.G. Akeroyd, A. Arhrib and M. Capdequi Peyranère, *Mod. Phys. Lett. A* **14** (1999) 2093.
- [21] S. Heinemeyer, W. Hollik and G. Weiglein, *J. High Ener. Phys.* **0006** (2000) 009.
- [22] DELPHI: LEPC talks, Presentations on Nov 9 1999, (http://delphiwww.cern.ch/öffline/physics_links/lepc.html)
- [23] V. Barger, M.S. Berger and P. Ohmann, *PRD* **47** (1093) 1993; M. Carena, M. Olechowski, S. Pokorski and C.E.M. Wagner, *Nucl. Phys. B* **426** (269) 1994.
- [24] S.H. Zhu, (hep-ph/9901221).
- [25] J.M. Cornwall, D.N. Levin and G. Tiktopoulos, *Phys. Rev. Lett.* **30** (1973) 1268; *Phys. Rev. D* **10** (1974) 1145; B.W. Lee, C. Quigg and H.B. Thacker, *Phys. Rev. D* **16** (1977) 1519.
- [26] M.S. Chanowitz and M.K. Gaillard, *Nucl. Phys. B* **261** (1985) 379; H. Veltman, *Phys. Rev. D* **41** (1990) 2294; J. Bagger and C. Schmidt, *Phys. Rev. D* **41** (1990) 264; H.-J. He, Y.-P. Kuang and X. Li, *Phys. Rev. Lett.* **69** (1992) 2619; *Phys. Rev. D* **49** (1994) 4842.
- [27] K. Odagiri, private communication.
- [28] K. Odagiri, *Phys. Lett. B* **452** (1999) 327.
- [29] A. Arhrib, M. Capdequi Peyranère, W. Hollik and G. Moutaka, (hep-ph/9912527).
- [30] G. Passarino and M. Veltman, *Nucl. Phys. B* **160** (1979) 151.

TABLE CAPTION

Table 1: The list of the kinematical factors $K_{i,\tau}(k, \bar{k}, \bar{\lambda})$.

FIGURE CAPTIONS

Fig. 1: The diagrams for $e^+e^- \rightarrow H^-W^+$. The circles in (a), and (b) represent all one-loop diagrams relevant to the HWV vertices ($V = \gamma, Z^0$) and the HW mixing. The arrows on the H^\pm bosons and the W boson lines indicate the flow of negative electric charge.

Fig. 2: The HWV vertices ($V = \gamma, Z^0$). The arrows on the H^\pm boson and the W boson lines indicate the flow of negative electric charge.

Fig. 3: The total cross section of $e^+e^- \rightarrow H^-W^+$ for $m_{H^\pm} = 200$ GeV at $\sqrt{s} = 500$ GeV as a function of $\tan\beta$ in the 2HDM (solid lines) and in the MSSM (dashed line). For the 2HDM, three solid curves correspond to $m_{A^0} = 300, 600$ and 1200 GeV. The other parameters are chosen as $\alpha = \beta - \pi/2$, $m_{h^0} = 120$ GeV, $m_{H^0} = 210$ GeV and $M = 0$ GeV.

Fig. 4: The \sqrt{s} dependence of the total cross section of $e^+e^- \rightarrow H^-W^+$ for $m_{H^\pm} = 200$ GeV for various $\tan\beta$ in the non-SUSY 2HDM. Solid curves are $\tan\beta = 0.3, 0.5, 1, 2, 4$ and dotted curves are $\tan\beta = 8, 16, 32$. The other parameters are chosen as $\alpha = \beta - \pi/2$, $m_{h^0} = 80$ GeV, $m_{H^0} = 210$ GeV, $m_{A^0} = 1200$ GeV and $M = 0$ GeV.

Fig. 5: The upper bound of the cross section of $e^+e^- \rightarrow H^-W^+$ for $m_{H^\pm} = 200$ GeV at $\sqrt{s} = 500$ GeV as a function of $\tan\beta$ under the conditions (34) and (35) in the non-SUSY 2HDM (solid curve). The dotted curve represent the cross section where the condition (35) is switched off. The dashed curve represent the cross section where only t - b loop contributions are included.

Fig. 6: The possible enhancement of the total cross section of $e^+e^- \rightarrow H^-W^+$ for various m_{H^\pm} at $\sqrt{s} = 500$ GeV as a function of $\tan\beta$ in the non-SUSY 2HDM under the conditions (34) and (35).

Fig. 7(a) The first group of the Feynman diagrams (the 't Hooft-Feynman gauge) of the HWV vertices ($V = \gamma, Z^0$), which corresponds to $X^{HWV(a)}$ ($X = F, G$ and H) in Appendix A. 1.

Fig. 7(b) The second group of the Feynman diagrams (the 't Hooft-Feynman gauge) of the HWV vertices ($V = \gamma, Z^0$), which corresponds to $X^{HWV(b)}$ ($X = F, G$ an H) in Appendix A. 1.

Fig. 7(c) The third group of the Feynman diagrams (the 't Hooft-Feynman gauge) of the HWV vertices ($V = \gamma, Z^0$), which corresponds to $X^{HWV(c)}$ ($X = F, G$ an H) in Appendix A. 1.

	$K_{1,\tau}(k, \bar{k}, \bar{\lambda})$	$K_{2,\tau}(k, \bar{k}, \bar{\lambda})$	$K_{3,\tau}(k, \bar{k}, \bar{\lambda})$
$\bar{\lambda} = 0$	$-\frac{1}{2m_W}(s - m_{H^\pm}^2 + m_W^2) \sin \Theta$	$\frac{1}{2} \frac{s^2}{m_W^3} \beta_{HW}^2 \sin \Theta$	0
$\bar{\lambda} = \pm$	$\sqrt{\frac{s}{2}}(\mp \cos \Theta + \tau)$	0	$-\frac{s}{m_W^2} \sqrt{\frac{s}{2}} \beta_{HW} (\cos \Theta \mp \tau)$

Table 1

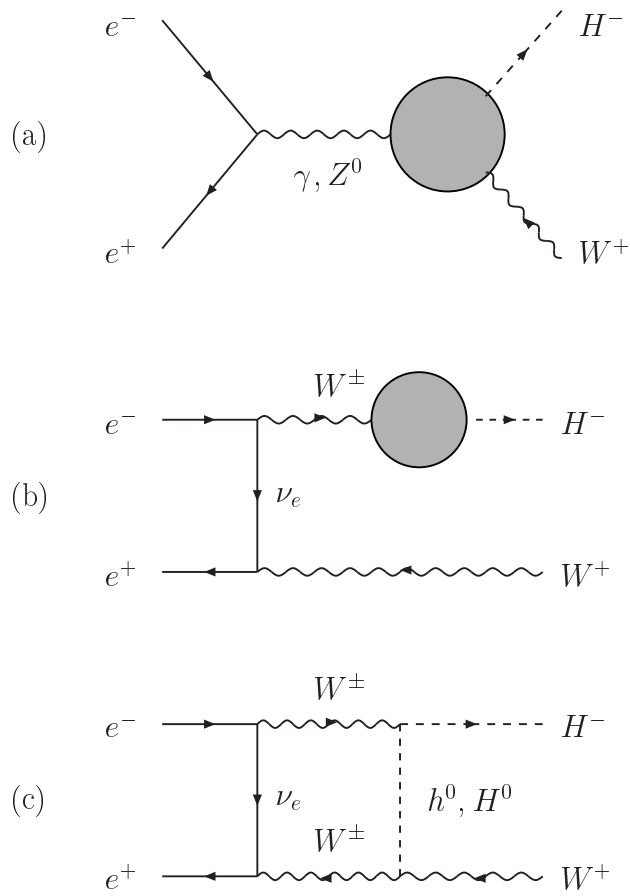
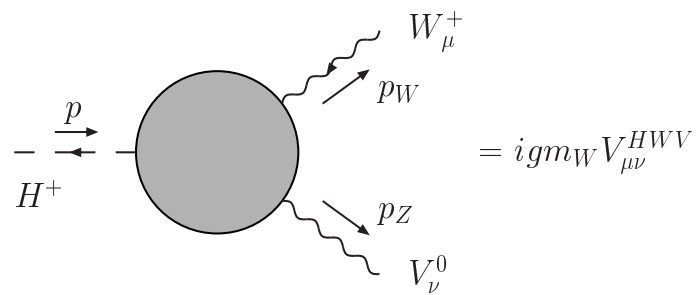


Figure 1



1

Figure 2

$$\sigma(e^-e^+ \rightarrow H^-W^+)$$

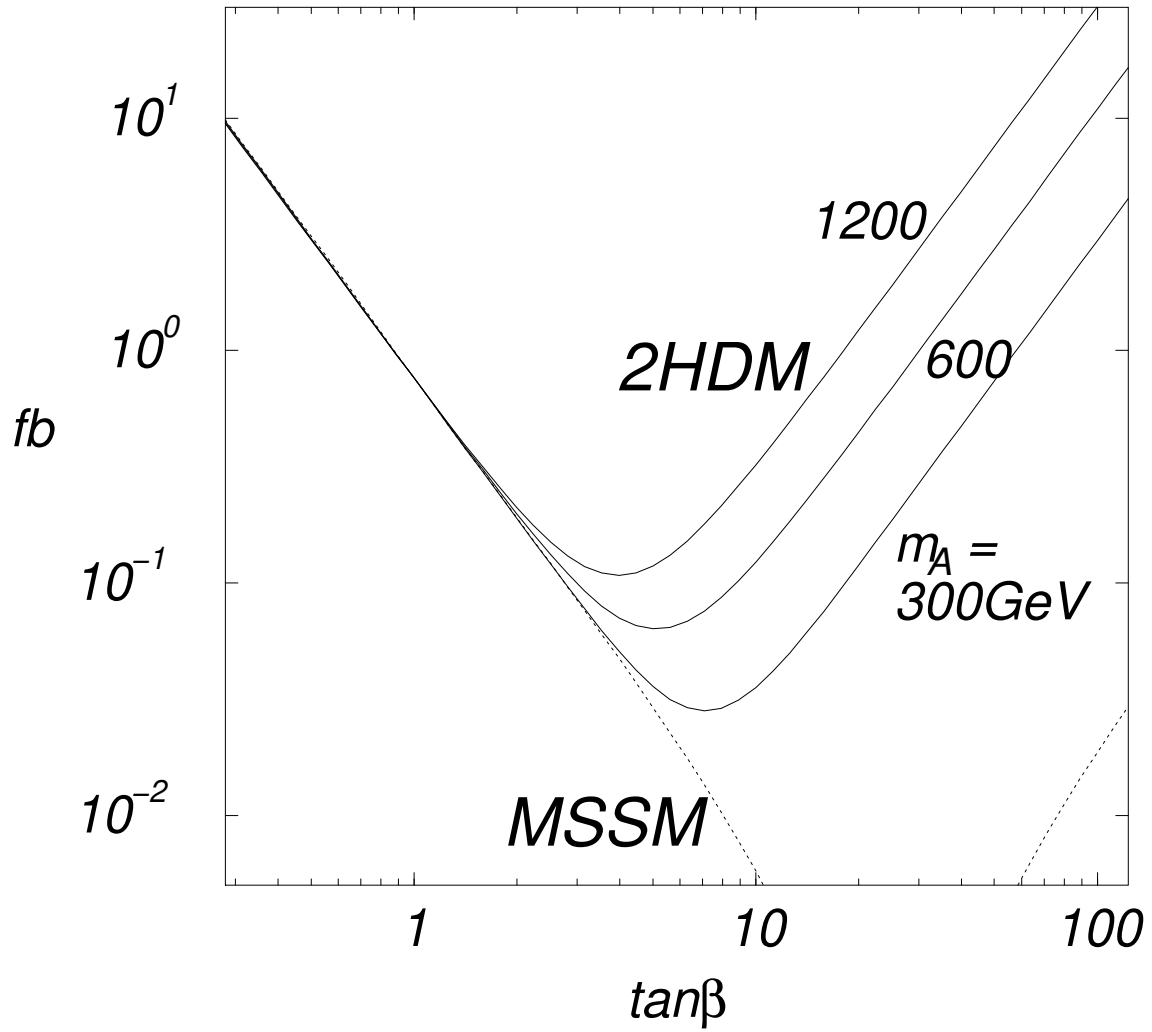


Figure 3

$$\sigma(e^-e^+ \rightarrow H^-W^+)$$

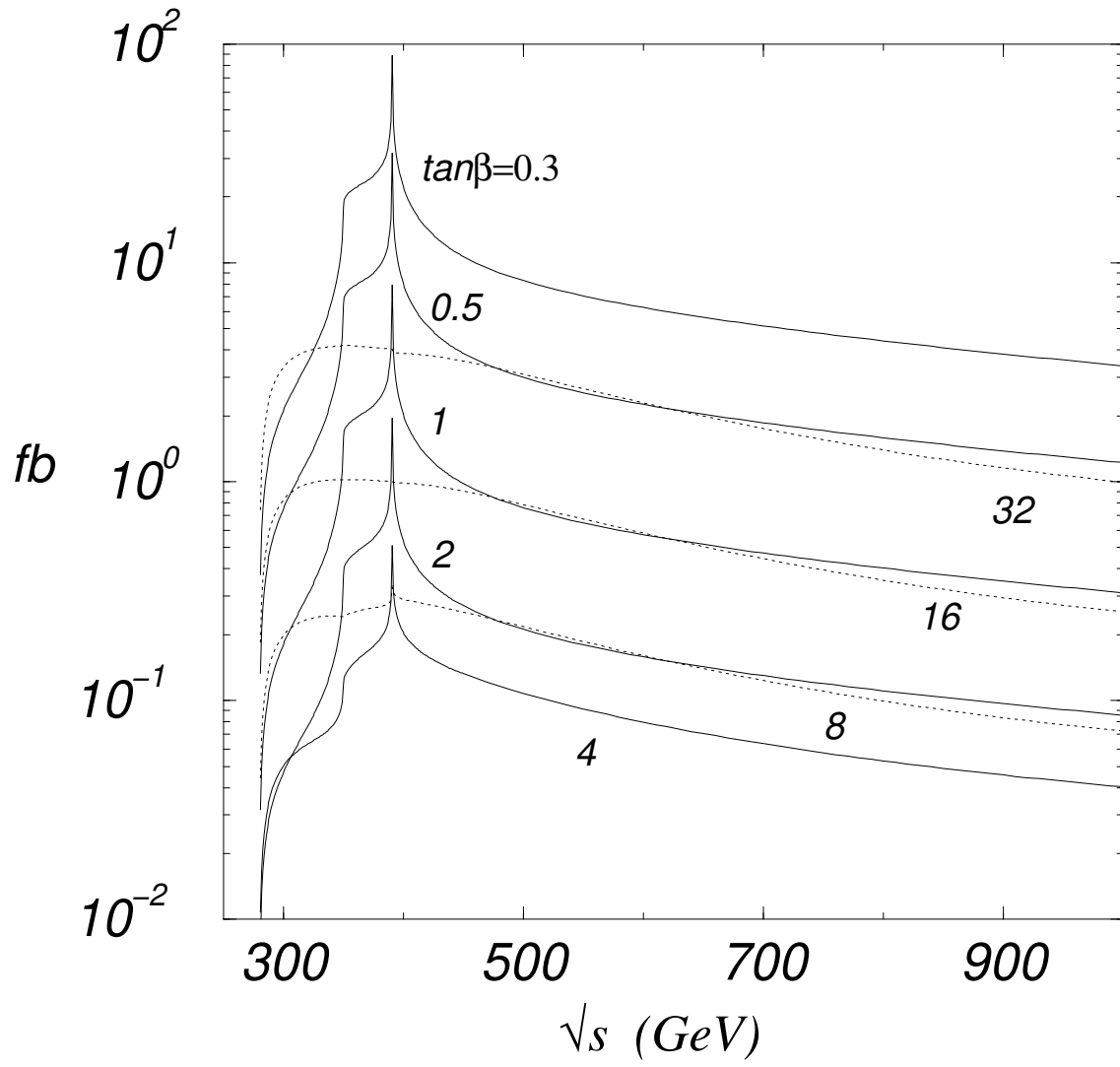


Figure 4

$$\sigma(e^-e^+ \rightarrow H^-W^+)$$

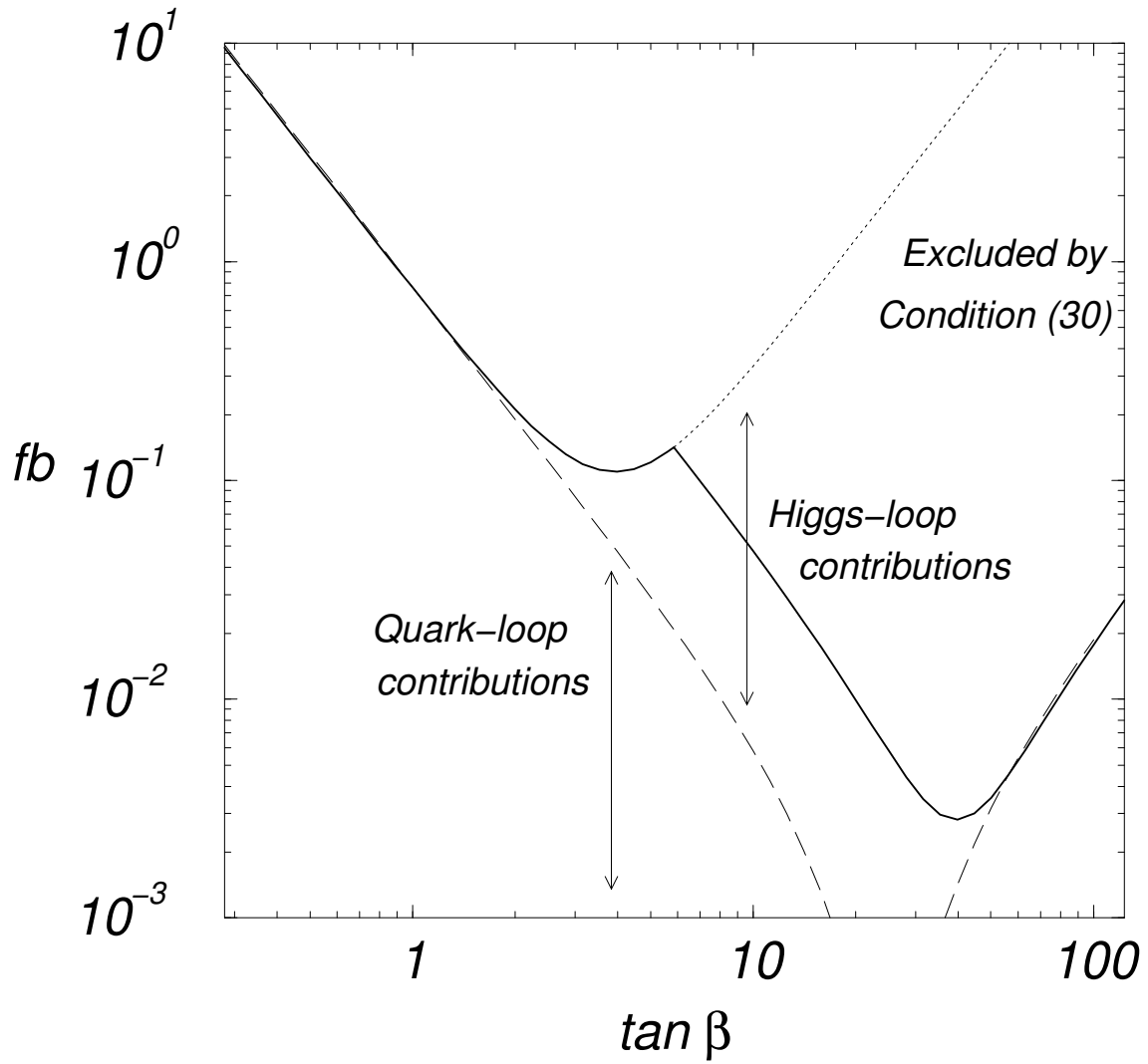


Figure 5

$$\sigma(e^-e^+ \rightarrow H^-W^+)$$

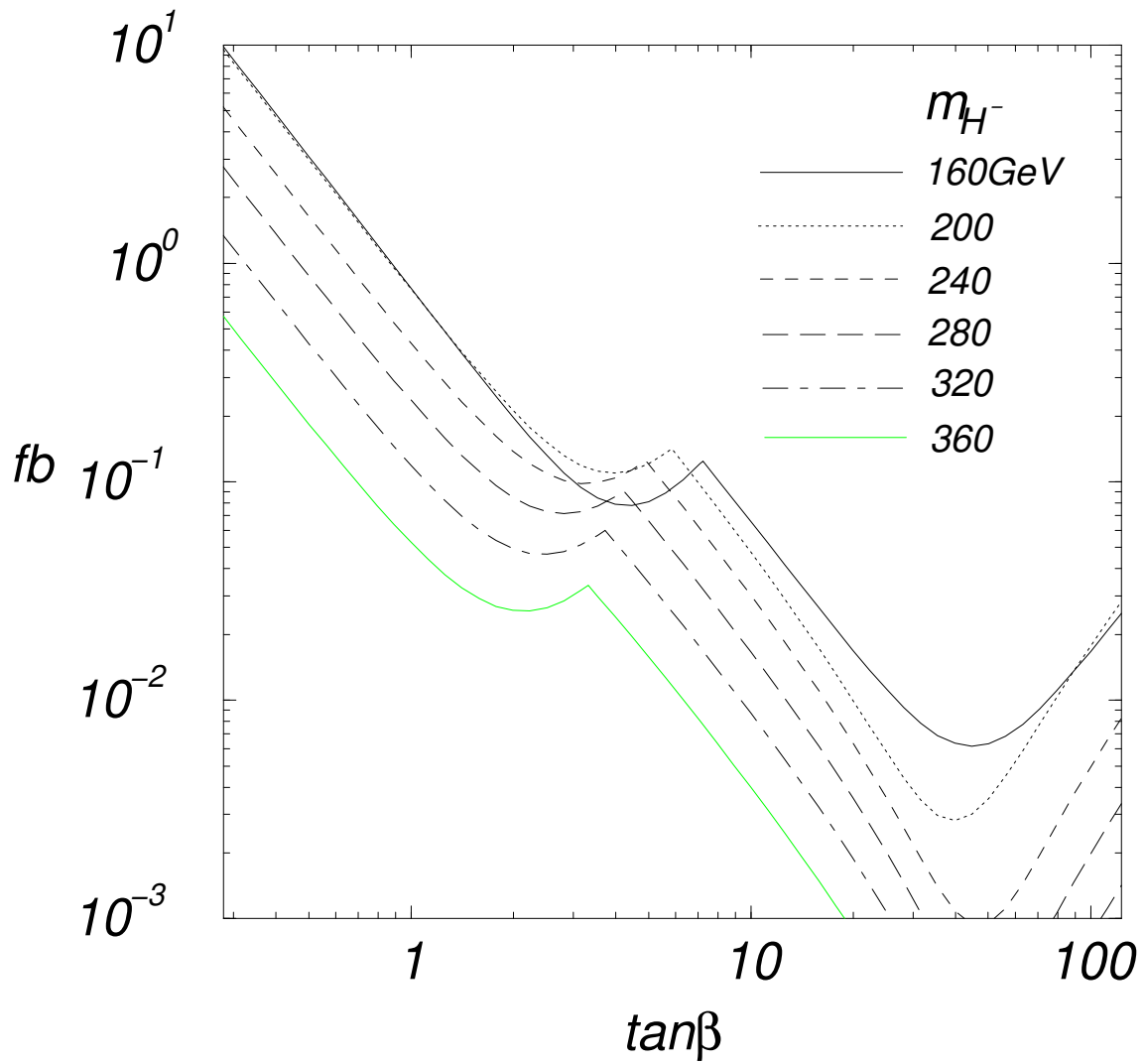
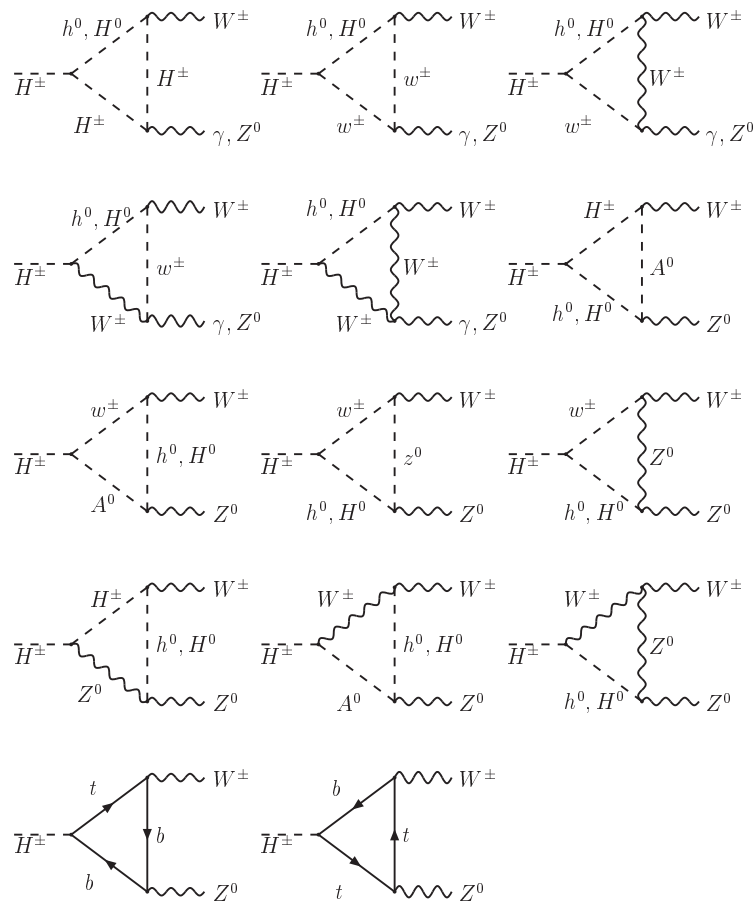


Figure 6



1

Figure 7(a)

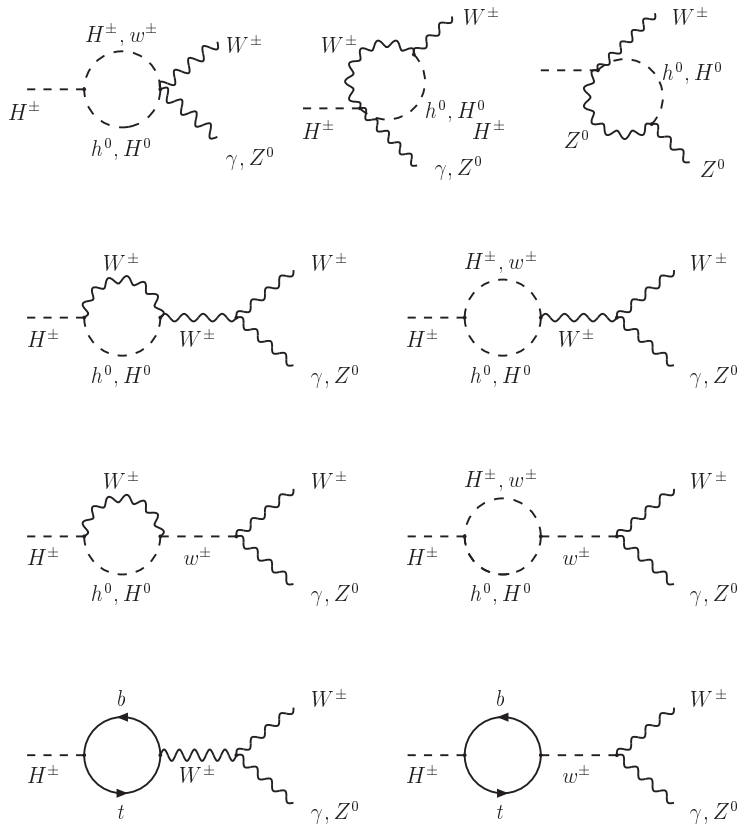
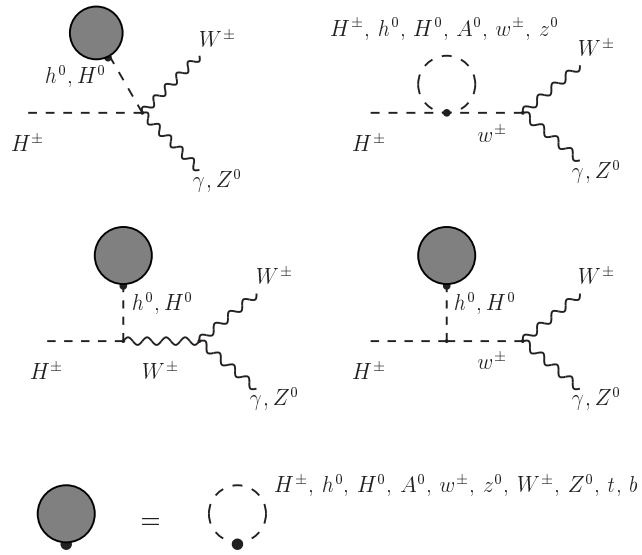


Figure 7(b)



1

Figure 7(c)